International Journal of Solids and Structures 264 (2023) 112093

Contents lists available at ScienceDirect

International Journal of Solids and Structures

journal homepage: www.elsevier.com/locate/ijsolstr

# A comparative study of analytical and numerical models for the elastic behavior of composites reinforced by coated unidirectional fibers

Helmut J. Böhm

*Institute of Lightweight Design and Structural Biomechanics, TU Wien, Gumpendorfer Straße 7, Vienna, A–1060, Austria*

ARTICLE INFO

*MSC:*
74A40
74E30
74M25
74Q05

*Keywords:*
Fiber reinforced composites
Coated fibers
Interphases
Elasticity

ABSTRACT

A number of continuum mechanical models for the macroscopic and microscopic linear elastic behavior of composites reinforced by continuous, unidirectional, coaxially coated fibers are critically compared. For the study, the interphase is assumed to be of finite thickness and uniform. Selected analytical mean-field methods and Finite-Element-based periodic homogenization models are applied to obtaining predictions for the effective elastic tensors and moduli of generic composites of this type. In addition, the phase-averaged microscopic stresses are evaluated for some macroscopic load cases. By comparing these results modeling schemes capable of providing high-quality predictions are identified.

## 1. Introduction

In many composites reinforced by unidirectional, continuous fibers a distinct layer of finite thickness, known as an interphase or mesophase, is present between fiber and matrix. This layer may result from chemical interactions between the constituents or it may be specifically engineered with the aim of modifying some aspects of the behavior of the composite. In the 2000s the latter issue has started to come to the forefront, compare, e.g., Jones (2010), Karger-Kocsis et al. (2015), Livanov et al. (2016) or Zheng et al. (2022). Recent relevant developments include "fuzzy fibers" coated with carbon nanotubes, see, e.g., Sager et al. (2009), and electrolyte coated carbon fibers for multifunctional composites, compare, e.g., Asp and Greenhalgh (2014). Such developments have fueled continuing research interest in models for predicting the effects of interphases on the behavior of continuously reinforced composites.

In the present work a number of continuum mechanical methods for modeling the elastic responses of idealized composites reinforced by coated, continuous, aligned fibers are critically compared and assessed. For this purpose the interphases are assumed to be uniform and of constant thickness, the fibers are taken to show a circular cross section, constituents are treated as perfectly bonded, and small strain, linear elastic behavior is considered. The comparisons are carried out for four sets of generic material parameters chosen to explore a wide range of elastic contrasts. Various configurations in terms of the volume fractions of the phases are studied.

Composites falling within the above scope show transversally isotropic macroscopic behavior, so that, in general, five independent elastic moduli are required for fully describing the effective elasticity tensor. The following short discussion of the state of the art concentrates on models that can provide predictions for the macroscopic elasticity tensors (or for appropriate sets of effective elastic moduli) of the composites. It is limited to developments that are directly relevant to the present study and is not intended as a formal review.

The majority of pertinent analytical approaches have used the concept of describing coated fibers via uniform, equivalent inhomogeneities, a strategy referred to as the "replacement method" by Hashin (1972). Modeling schemes of this type can be used to describe the effects of interphases of finite as well as interfaces of vanishing thickness, compare, e.g., Firooz et al. (2021) and Duan et al. (2022). Most of the two-step methods for coated fibers resulting from replacement schemes can be classified as falling into two distinct lines of development.

The first group of models are based on rigorous elasticity solutions for the displacement, stress and strain fields in a coated cylinder embedded in a matrix. Early works of this type, e.g., Theocaris and Varias (1986), provided solutions for some, but not all, of the required moduli. The full set of "auxiliary problems" necessary for obtaining complete sets of transversally isotropic, thermoelastic moduli describing such configurations was explicitly spelt out by Benveniste et al. (1989).

*E-mail address:* hjb@ilsb.tuwien.ac.at.
*URL:* https://www.ilsb.tuwien.ac.at/~hjb.

https://doi.org/10.1016/j.ijsolstr.2022.112093
Received 15 July 2022; Received in revised form 4 December 2022; Accepted 19 December 2022
Available online 22 December 2022

## Nomenclature

### Acronyms

| | |
|---|---|
| BIR | Birman's model (Birman, 2021) |
| CCA | Composite Cylinder Assemblage (Hashin and Rosen, 1964) |
| DIM | Double Inclusion Method (Hori and Nemat-Nasser, 1993) |
| DIMM | DIM dilute solution plus Mori–Tanaka Method |
| EDS | Exact dilute solution plus Differential Scheme |
| EGSC | Exact dilute solution plus Generalized Self-Consistent scheme |
| EHS | Exact dilute solution plus Hashin–Shtrikman bounds |
| EHSW | Exact dilute solution plus two-phase Hashin–Shtrikman–Willis bounds |
| EMCM | Exact dilute solution plus Method of Conditional Moments |
| EMT | Exact dilute solution plus Mori–Tanaka methods |
| E3PB | Exact dilute solution plus 3-Point Bounds |
| E3PE | Exact dilute solution plus 3-Point Estimates |
| HMM | Hierarchical Multi-interphase Model (Li et al., 2011) |
| HSW | three-phase Hashin–Shtrikman–Willis bounds |
| FEM | Finite Element Method |
| GEEE | General Explicit Eshelby-type Estimator (Ghazavizadeh et al., 2019) |
| MTM | Mori–Tanaka Method (Benveniste, 1987) |
| MTDS | Mori–Tanaka dilute solution plus Differential Scheme |
| MTMT | Mori–Tanaka dilute solution plus Mori–Tanaka method |
| PHA | Periodic Hexagonal Array (of fibers) |
| PMC | Periodic Multi-fiber Cell |
| RDIM | Reformulated Double Inclusion Model (Dinzart et al., 2016) |
| RVE | Representative Volume Element |

### Symbols

| | |
|---|---|
| $\bar{\mathbf{A}}$ | (phase averaged) strain concentration tensor |
| $\bar{\mathbf{B}}$ | (phase averaged) stress concentration tensor |
| $\mathbf{C}$ | compliance tensor |
| $\mathbf{E}$ | elasticity tensor |
| $\mathbf{I}$ | 4th order unit tensor |
| $\mathbf{L}$ | tensor providing information on two-point statistics (Khoroshun et al., 1988) |
| $\mathbf{P}$ | Hill (mean polarization factor) tensor |
| $\mathbf{S}$ | Eshelby tensor |
| $\bar{\mathbf{T}}$ | (phase averaged) partial strain concentration tensor |
| $\boldsymbol{\varepsilon}$ | strain tensor |
| $\boldsymbol{\sigma}$ | stress tensor |
| $E$ | Young's modulus |
| $G$ | shear modulus |
| $K$ | bulk modulus |
| $\nu$ | Poisson number |
| $\Omega$ | volume |
| $\xi$ | phase volume fraction |
| $\eta$ | partial volume fraction of core or layer |
| $a$ | (minor) in-plane side length of a volume element |
| $t$ | thickness of the interphase |

### Subscripts, superscripts and brackets

| | |
|---|---|
| $\bullet^{(p)}$ | phase in general |
| $\bullet^{(m)}$ | matrix |
| $\bullet^{(c)}$ | fiber core |
| $\bullet^{(l)}$ | coating layer / interphase |
| $\bullet^{I}$ | equivalent uniform inhomogeneity |
| $\bullet^{*}$ | effective / macroscopic |
| $\bullet^{(0)}$ | reference medium |
| $\bullet_{A}$ | axial |
| $\bullet_{T}$ | transverse |
| $\bullet_{dil}$ | dilute |
| $\bullet_{eqv}$ | equivalent |
| $\langle\bullet\rangle$ | volume average |

Appropriate models were proposed, e.g., by Pagano and Tandon (1988), Hashin (1990) or Benveniste et al. (1989); the latter contribution approximated the macroscopic responses via a Mori–Tanaka method. Hervé and Zaoui (1995) started out from the displacement solutions for the Navier equations in cylindrical coordinates and used the interfacial continuity conditions to set up a transfer matrix formalism for the coefficients of the ansatz terms. On this basis expressions for all effective moduli of the non-dilute composite were set up, the effective transverse shear modulus being obtained by equating the strain energies in the composite and in the equivalent homogeneous embedding medium (Christensen and Lo, 1979). Hervé-Luanco (2020) provided simplified expressions for the Hervé/Zaoui self-consistent model and Blondel et al. (2020) extended it to studying morphological fluctuations in composites reinforced by coated fibers. Wang et al. (2016) as well as Chatzigeorgiou and Meraghni (2019) used analogous ansatz functions to evaluate explicit, rigorous expressions for the phase averaged concentration factors pertaining to single fiber–interphase systems embedded in an infinite matrix. It is worth noting that dilute solutions of this type are available only for concentrically coated spheres and for coaxially coated, infinitely long cylinders.

The second group of models aim at providing analytical approximations for dilute, coated configurations on the basis of the Eshelby tensor (Eshelby, 1957) which, per se, is limited to handling uniform inhomogeneities. This modeling strategy was pioneered by the Double Inclusion Model (DIM) of Hori and Nemat-Nasser (1993), which provides expressions for the elasticity and concentration tensors of the equivalent inhomogeneities. These results were combined with a Mori–Tanaka method by Dunn and Ledbetter (1995) to provide estimates for the macroscopic elastic responses of non-dilute composites containing aligned, coated reinforcements. Aboutajeddine and Neale (2005) proposed an improved version of the DIM. This formed the basis for a Generalized Self-Consistent scheme for the effective elastic behavior of materials reinforced by coated ellipsoidal fibers or particles proposed by Dinzart et al. (2016), referred to as the Reformulated Double Inclusion Model (RDIM). In an alternative line of development Eshelby-tensor-based micromechanics theories have been deployed for describing dilute inhomogeneity–coating arrangements. The use of Mori–Tanaka-type methods for modeling the behavior of equivalent coated inhomogeneities seems to go back to Friebel et al. (2006), who considered a number of three-phase schemes in viscoelasticity. Recently, Ghazavizadeh et al. (2019) presented a hierarchical approach to studying composites containing multiply coated reinforcements, called the General Explicit Eshelby-Type Estimator (GEEE). This can be interpreted as a succession of steps each of which uses the

Hashin–Shtrikman estimates of Ponte Castañeda and Willis (1995); for the case of a uniform, coaxial coating it reduces to two Mori–Tanaka steps. The GEEE was shown by its authors to give identical results to the RDIM of Dinzart et al. (2016). Using a Differential Scheme for evaluating the properties of the equivalent fibers was proposed by Sevostianov et al. (2012), whereas Liu and Bian (2019) developed a two-step model employing dilute concentration tensors based on an effective field method. Most models in this group are capable of providing predictions for ellipsoidal core–interphase configurations that do not have to be homothetic. Coaxially coated, circular cylinders are a special case of such geometries.

Eshelby tensors may also be used within one-step models for elastic composites containing coated, ellipsoidal reinforcements, an example being the approximation proposed by Birman (2021). A further approach to studying the effects of coated ellipsoidal inhomogeneities makes use of the interfacial operator proposed by Hill (1983). This line of work was initiated by Cherkaoui et al. (1994) for handling thin interphases and underwent considerable development. For example, a Generalized Self-Consistent scheme for general configurations was reported by Berbenni and Cherkaoui (2010) to closely approach results based on rigorous solutions.

A conceptually different path towards obtaining closed form solutions for the responses of fiber reinforced composites with uniform interphases was proposed by Guinovart-Díaz et al. (2005), who applied an analytical asymptotic homogenization scheme to Periodic Hexagonal Arrays (PHA) of coated fibers.

Numerical work on the behavior of elastic composites reinforced by continuous, aligned, coated fibers started to appear in the literature in the late 1980s. At first it concentrated on the responses to transverse loading, using the Finite Element Method (FEM) and the Boundary Element Method for studying planar, periodic hexagonal or periodic square arrays of coated fibers, see, e.g., Adams (1987) and Achenbach and Zhu (1990). Among the first numerics-based publications providing effective elastic tensors of such composites was a study by Gardner et al. (1993), who applied the Method of Cells to describing periodic square arrays of coated fibers of square cross-section.

Most of the numerical works pertinent to the present focus have combined periodic homogenization schemes with the FEM. Chouchaoui and Benzeggagh (1997) reported the effective elastic tensors of a glass–epoxy bundle using PHA microgeometries, as did Hammerand et al. (2007) for periodic hexagonal as well as clustered arrangements of hollow fibers. Periodic volume elements containing a number of randomly positioned reinforcements, which are a mainstay of numerical micromechanics of composite materials and are referred to as Periodic Multi-fiber Cells (PMC) in the following, were first applied to extracting the effective elasticity tensors of materials reinforced by coated unidirectional fibers by Kari et al. (2008). Volume elements of this type were also employed, e.g., by Gusev and Kern (2018) in a viscoelastic setting and by Pitchai et al. (2020) in combination with the Variational Asymptotic Method.

Other numerical schemes suitable for evaluating the effective elastic tensors of materials reinforced by coated unidirectional fibers include Fast Fourier Transformation methods for periodic models, compare Wang et al. (2019), as well as multipole expansions or FE-based homogenization schemes that employ macrohomogeneous boundary conditions, compare Mogilevskaya et al. (2010) and Riaño et al. (2018), respectively. Their use, however, seems to have been limited to planar models.

Neither numerical models based on discrete volume elements nor analytical methods can provide exact solutions for the effective elastic responses of non-dilute composites reinforced by (non-coated or coated) unidirectional, continuous fibers. These two groups of modeling strategies, however, make use of fundamentally different approximations in order to obtain estimates. Whereas typical analytical schemes combine statistical descriptions of phase geometries with mean field or effective field approximations for the microfields in the constituents, the numerical approaches are "full-field models" that can resolve the stress and strain fields of specific microgeometries at high accuracy. These phase arrangements, however, in practice are only approximations to proper Representative Volume Elements (RVEs) as defined by Hill (1963). On account of the marked differences underlying these approaches consistent agreement between given analytical and numerical methods, maintained over sets of dissimilar input data, is a strong indicator that both results are valid. Also, in view of the computational costs of numerical models, identifying high-quality analytical approximations is of obvious practical interest.

A number of studies in the literature have included comparisons between different models for the elastic responses of composites reinforced by coated unidirectional fibers, see, e.g., Wang et al. (2016), Chatzigeorgiou and Meraghni (2019) or Chen et al. (2021). Further relevant information can be obtained from the other publications referenced above. The present work aims at systematically extending this body of knowledge, special emphasis being put on models introduced during the past decade. It follows the strategy used for comparing models for materials reinforced by coated spheres by Böhm (2019), where analytical and numerical schemes are assessed for a number of geometrical configurations and generic phase properties.

Basics of the analytical and numerical modeling approaches used in the paper are introduced in Section 2, expressions for some of the analytical sub-models being provided in Appendix A. Section 3 presents and compares results obtained with the various models. Data on equivalent homogeneous fibers are presented in Appendix B and the behavior of some pertinent bounds is discussed in Appendix C. The supplementary material provides tables of predictions for effective and equivalent moduli as well as for phase-averaged microstresses.

## 2. Models

In this section the basic ideas of two-step analytical approaches as well as the numerical schemes are discussed. All models considered are based on stress equilibrium in multi-phase regions.

### 2.1. Two-step analytical mean-field models

The present contribution deals with linear elastic multi-phase materials the macroscopic behavior of which takes the form

$$\langle\boldsymbol{\sigma}\rangle = \mathbf{E}^*\langle\boldsymbol{\varepsilon}\rangle \quad \text{and} \quad \langle\boldsymbol{\varepsilon}\rangle = \mathbf{C}^*\langle\boldsymbol{\sigma}\rangle \quad , \tag{1}$$

where $\langle\boldsymbol{\sigma}\rangle$ and $\langle\boldsymbol{\varepsilon}\rangle$ are the macroscopic stress and strain tensors, $\mathbf{E}^*$ is the effective elasticity tensor and $\mathbf{C}^*$ the effective compliance tensor. The constitutive behavior of each phase $^{(\mathrm{p})}$ can be denoted in analogy as

$$\langle\boldsymbol{\sigma}\rangle^{(\mathrm{p})} = \mathbf{E}^{(\mathrm{p})}\langle\boldsymbol{\varepsilon}\rangle^{(\mathrm{p})} \quad \text{and} \quad \langle\boldsymbol{\varepsilon}\rangle^{(\mathrm{p})} = \mathbf{C}^{(\mathrm{p})}\langle\boldsymbol{\sigma}\rangle^{(\mathrm{p})} \quad , \tag{2}$$

where $\langle\boldsymbol{\varepsilon}\rangle^{(\mathrm{p})}$ and $\langle\boldsymbol{\sigma}\rangle^{(\mathrm{p})}$ stand for the volume averages of the stress and strain tensors, respectively, in phase $^{(\mathrm{p})}$. The relations

$$\langle\boldsymbol{\sigma}\rangle = \sum_{(\mathrm{p})} \xi^{(\mathrm{p})}\langle\boldsymbol{\sigma}\rangle^{(\mathrm{p})} \quad \text{and} \quad \langle\boldsymbol{\varepsilon}\rangle = \sum_{(\mathrm{p})} \xi^{(\mathrm{p})}\langle\boldsymbol{\varepsilon}\rangle^{(\mathrm{p})} \quad , \tag{3}$$

follow directly from volume averaging, $\xi^{(\mathrm{p})}$ being the volume fraction of phase $^{(\mathrm{p})}$.

Mean-field micromechanical methods in elasticity can be conveniently formulated in terms of phase-averaged strain and stress concentration tensors (Hill, 1963), $\bar{\mathbf{A}}^{(\mathrm{p})}$ and $\bar{\mathbf{B}}^{(\mathrm{p})}$, which connect the volume averaged stresses and strains to their macroscopic equivalents, such that

$$\langle\boldsymbol{\varepsilon}\rangle^{(\mathrm{p})} = \bar{\mathbf{A}}^{(\mathrm{p})}\langle\boldsymbol{\varepsilon}\rangle \quad \text{and} \quad \langle\boldsymbol{\sigma}\rangle^{(\mathrm{p})} = \bar{\mathbf{B}}^{(\mathrm{p})}\langle\boldsymbol{\sigma}\rangle \quad . \tag{4}$$

The closely related partial strain concentration tensors, which link the phase averaged strains in two different phases, $^{(\mathrm{p})}$ and $^{(\mathrm{q})}$, are defined as

$$\langle\boldsymbol{\varepsilon}\rangle^{(\mathrm{p})} = \bar{\mathbf{T}}^{(\mathrm{p,q})}\langle\boldsymbol{\varepsilon}\rangle^{(\mathrm{q})} \quad . \tag{5}$$

For a three-phase composite consisting of a matrix $^{(m)}$ and two inhomogeneity phases, $^{(c)}$ and $^{(l)}$, the relations

$$\xi^{(m)}\bar{\mathbf{A}}^{(m)} + \xi^{(c)}\bar{\mathbf{A}}^{(c)} + \xi^{(l)}\bar{\mathbf{A}}^{(l)} = \mathbf{I} \tag{6}$$

hold, where $\mathbf{I}$ stands for the 4th order unit tensor. The effective elasticity tensor of such a composite is given by

$$\mathbf{E}^{*} = \xi^{(m)}\mathbf{E}^{(m)}\bar{\mathbf{A}}^{(m)} + \xi^{(c)}\mathbf{E}^{(c)}\bar{\mathbf{A}}^{(c)} + \xi^{(l)}\mathbf{E}^{(l)}\bar{\mathbf{A}}^{(l)} \quad , \tag{7}$$

which, like Eq. (6), is a direct consequence of Eq. (3).

By setting

$$\eta^{(c)}\mathbf{E}^{(c)}\bar{\mathbf{A}}^{(c)} + \eta^{(l)}\mathbf{E}^{(l)}\bar{\mathbf{A}}^{(l)} = \mathbf{E}^{I}_{eqv}\bar{\mathbf{A}}^{I}_{eqv} \quad , \tag{8}$$

where the "partial volume fractions", $\eta^{(c)}$ and $\eta^{(l)}$, are defined as

$$\eta^{(c)} = \frac{\xi^{(c)}}{\xi^{(c)}+\xi^{(l)}} \quad \text{and} \quad \eta^{(l)} = \frac{\xi^{(l)}}{\xi^{(c)}+\xi^{(l)}} \quad , \tag{9}$$

Eq. (7) can be brought into the form

$$\mathbf{E}^{*} = \xi^{(m)}\mathbf{E}^{(m)}\bar{\mathbf{A}}^{(m)} + \xi^{I}\mathbf{E}^{I}_{eqv}\bar{\mathbf{A}}^{I}_{eqv} \quad . \tag{10}$$

$\mathbf{E}^{I}_{eqv}$ and $\bar{\mathbf{A}}^{I}_{eqv}$ can be interpreted as the elasticity and averaged strain concentration tensors, respectively, pertaining to uniform equivalent inhomogeneities of volume fraction $\xi^{I} = \xi^{(c)}+\xi^{(l)}$. The above definitions, which correspond to Hashin's replacement method, also imply that $\xi^{(c)} = \eta^{(c)}\xi^{I}$ and $\xi^{(l)} = \eta^{(l)}\xi^{I}$. In addition, consistency with Eq. (6) results in the requirement that

$$\bar{\mathbf{A}}^{I}_{eqv} = \eta^{(c)}\bar{\mathbf{A}}^{(c)} + \eta^{(l)}\bar{\mathbf{A}}^{(l)} \quad . \tag{11}$$

It is worth noting that Eqs. (6) to (11) hold for any three-phase composite regardless of its phase topology or geometry. Information on specific configurations, e.g., coated inhomogeneities consisting of a core $^{(c)}$ surrounded by an interphase layer $^{(l)}$, must be introduced via suitable concentration tensors $\bar{\mathbf{A}}^{(c)}$ and $\bar{\mathbf{A}}^{(l)}$.

In analytical micromechanics estimates for responses at finite reinforcement volume fractions are often based on the behavior of dilute systems such as single inhomogeneities embedded in an infinite matrix region. This strategy is directly applicable to composites reinforced by coated reinforcements that are described via equivalent, uniform inhomogeneities. On this basis a range of two-step schemes can be set up, in which the dilute, coated reinforcements embedded in the matrix are described via equivalent elasticity tensors $\mathbf{E}^{I}_{eqv}$ and/or strain concentration tensors $\bar{\mathbf{A}}^{I}_{dil,eqv}$ that are obtained from suitable *"equivalent homogeneous fiber sub-models"*. In the second step, essentially any micromechanical model applicable to two-phase composites, referred to as a *"composite-level sub-model"* in the following, may be used for the transition from dilute to non-dilute volume fractions. In such a "construction kit" approach the overall accuracy of any scheme necessarily depends on that of either of the sub-models.

For some analytical micromechanical models that are candidates for use at the composite level it is sufficient to know the equivalent elastic moduli of the coated fibers, examples being the third order weak contrast expansions ("three-point estimates") of Torquato (1998) or the Generalized Self-Consistent scheme of Christensen and Lo (1979). Conversely, if the dilute strain concentration tensors of core and coating as well as the non-dilute equivalent concentration tensor $\bar{\mathbf{A}}^{I}_{eqv}$ are known, the effective elasticity tensor may be obtained as

$$\begin{aligned}\mathbf{E}^{*} &= \mathbf{E}^{(m)} + \xi^{I}(\mathbf{E}^{(m)} - \mathbf{E}^{(l)})\,\bar{\mathbf{A}}^{I}_{eqv} + \xi^{(c)}(\mathbf{E}^{(c)} - \mathbf{E}^{(l)})\,\bar{\mathbf{A}}^{(l)}_{dil} \\ &= \mathbf{E}^{(m)} + \xi^{I}(\mathbf{E}^{(m)} - \mathbf{E}^{(c)})\,\bar{\mathbf{A}}^{I}_{eqv} + \xi^{(l)}(\mathbf{E}^{(l)} - \mathbf{E}^{(c)})\,\bar{\mathbf{A}}^{(c)}_{dil} \quad ,\end{aligned} \tag{12}$$

compare Dunn and Ledbetter (1995), no explicit expression for $\mathbf{E}^{I}_{eqv}$ being needed.

Many mean-field-type composite-level sub-models, however, require both $\mathbf{E}^{I}_{eqv}$ and $\bar{\mathbf{A}}^{I}_{dil,eqv}$, compare, e.g. Eqs. (A.4) and (A.5). A number of relations are available that provide links between these tensors. On the one hand, if the phase-level dilute concentration tensors $\bar{\mathbf{A}}^{(c)}_{dil} = \bar{\mathbf{T}}^{(c,m)}_{dil}$ and $\bar{\mathbf{A}}^{(l)}_{dil} = \bar{\mathbf{T}}^{(l,m)}_{dil}$ are known, as is the case for the exact solutions given by Wang et al. (2016) and Chatzigeorgiou and Meraghni (2019) or the DIM, $\bar{\mathbf{A}}^{I}_{dil,eqv}$ may be evaluated from the dilute equivalent of Eq. (11), as

$$\bar{\mathbf{A}}^{I}_{dil,eqv} = \eta^{(c)}\bar{\mathbf{A}}^{(c)}_{dil} + \eta^{(l)}\bar{\mathbf{A}}^{(l)}_{dil} \quad . \tag{13}$$

On the other hand, if the equivalent elasticity tensor, $\mathbf{E}^{I}_{eqv}$, is available, the equivalent dilute strain concentration tensor can be estimated from standard results for dilute two-phase configurations such as

$$\bar{\mathbf{A}}^{I}_{dil,eqv} = \left[\mathbf{I} + \mathbf{S}^{I,m}\mathbf{C}^{(m)}(\mathbf{E}^{I}_{eqv} - \mathbf{E}^{(m)})\right]^{-1} \tag{14}$$

(Hill, 1965). Here $\mathbf{S}^{I,m}$ is the Eshelby tensor pertaining to the shape of the compound inhomogeneity. Finally, equivalent elasticity tensors can be evaluated from the concentration tensors via Eq. (8) as

$$\mathbf{E}^{I}_{eqv} = \left(\eta^{(c)}\mathbf{E}^{(c)}\bar{\mathbf{A}}^{(c)}_{dil} + \eta^{(l)}\mathbf{E}^{(l)}\bar{\mathbf{A}}^{(l)}_{dil}\right)(\bar{\mathbf{A}}^{I}_{dil,eqv})^{-1} \quad , \tag{15}$$

provided $\bar{\mathbf{A}}^{I}_{dil,eqv}$ is invertible (which, in general, is the case for continuous, aligned fibers).

Whereas for two-phase composites the effective and phase elastic tensors uniquely determine the phase averaged concentration tensors, no such unambiguous relationships are available for general multiphase composites. However, by using the concept of equivalent inhomogeneities, composites reinforced by (simply or multiply) coated inhomogeneities can be treated as hierarchies of two-phase materials, so that all phase-level concentration tensors can be extracted once the effective elasticities are known, e.g.,

$$\begin{aligned}\bar{\mathbf{A}}^{I}_{eqv} &= \frac{1}{\xi^{I}}(\mathbf{E}^{I}_{eqv} - \mathbf{E}^{(m)})^{-1}(\mathbf{E}^{*} - \mathbf{E}^{(m)}) \\ \bar{\mathbf{A}}^{(c)} &= \frac{1}{\eta^{(c)}}(\mathbf{E}^{(c)} - \mathbf{E}^{(l)})^{-1}(\mathbf{E}^{I}_{eqv} - \mathbf{E}^{(l)})\bar{\mathbf{A}}^{I}_{eqv} \quad ,\end{aligned} \tag{16}$$

compare Böhm (2019). Furthermore, it is possible to evaluate the stress concentration tensors of the phases and of the equivalent inhomogeneity from the corresponding strain concentration tensors (and vice versa) by postprocessing operations of the type

$$\bar{\mathbf{B}}^{(p)} = \mathbf{E}^{(p)}\bar{\mathbf{A}}^{(p)}[\mathbf{E}^{*}]^{-1} \quad , \tag{17}$$

see Dvorak (1991). A number of additional relations (pertaining, e.g., to thermoelasticity) given by Böhm (2019) for materials containing coated spherical particles also hold for composites reinforced by unidirectional, coated fibers.

Composites of the type considered in the present study are a special type of three-phase material. Accordingly, they must fulfill the appropriate three-phase Hashin–Shtrikman–Willis bounds (Willis, 1977). Furthermore, it is possible to exploit the equivalent inhomogeneities to set up two-phase Hashin–Shtrikman bounds (Hashin, 1965, 1983), Hashin–Shtrikman–Willis bounds or three-point bounds (Torquato, 2002).

### 2.2. Numerical models

Volume-discretizing numerical methods tend to become unwieldy when applied to studying microgeometries incorporating very thin interphases — resolving fine geometrical features quickly leads to very large models. The Finite Element Method used here, with its inherent capability of handling unstructured meshes and, consequently, of local mesh refinement, can mitigate this practical difficulty to a considerable extent. Nevertheless, models of the type discussed in this section are not very efficient for partial interphase volume fractions significantly lower than, say, $\eta^{(l)} = 0.05$. This issue poses less of a constraint when an appropriate Boundary Element Method is used.

The numerical models employed in the present work evaluate the elastic responses of two types of three-dimensional volume element. These are, on the hand, Periodic Hexagonal Arrays (PHA) of fibers, which combine geometrical simplicity with the required transversally isotropic elastic symmetry, compare Ptashnyk and Seguin (2016), and,

on the other hand, Periodic Multi-fiber Cells (PMC) that contain a considerable number of randomly positioned, identical, aligned, cylindrical fibers. The method of macroscopic degrees of freedom (Michel et al., 1999), a standard periodic homogenization approach, was applied to the volume elements. The latter have the shape of right hexahedra, see Fig. 1. The thickness of the cells was set to $0.02a$, where $a$ is the minor in-plane side length of the volume element. PMC arrangements containing 50 fibers each were generated by an in-house code using random sequential addition followed by random perturbation, which allows reaching fiber volume fractions exceeding 0.7. The minimum distances between individual fibers and between the cylinders' surfaces and the faces of the volume elements were thresholded at $0.01a$ and $0.015a$, respectively. Coaxial cylindrical cores were inscribed into the cylindrical inhomogeneities, with the regions between the two cylinders representing the coating layer. Alternatively, the interphases of closely approaching fibers may be treated as confluent, compare, e.g., Riaño et al. (2018); such geometries, however, are less directly comparable to the ones underlying the analytical models.

For an interphase partial volume fraction of $\eta^{(\mathrm{I})} = 0.1$ and a volume element containing 50 cylindrical fibers at a volume fraction of $\xi^{\mathrm{I}} = 0.2$, the interphase thickness evaluates as $t \approx 0.0018a$. Geometries become more benign in this respect with increasing $\xi^{\mathrm{I}}$ and $\eta^{(\mathrm{I})}$. Meshing was carried out with the preprocessor `netgen` (Schöberl, 1997), which has strong capabilities in generating graded meshes. Tetrahedral continuum elements with quadratic interpolation were used throughout the study. For interphase partial volume fractions of $\eta^{(\mathrm{I})} \geq 0.1$ the meshes were required to incorporate at least two elements over the layer's thickness in order to allow resolving stress and strain distributions sufficiently well. For the analyses with $\eta^{(\mathrm{I})} = 0.05$, however, only one element over the coating thickness could be accommodated within models of acceptable size. The resulting node counts in the meshes for the periodic multi-fiber cells range between $1.3\times10^6$ and $8.7\times10^6$, depending on the fiber volume fraction and the interphase thickness, whereas they are lower by considerably more than an order of magnitude for the PHA unit cells. Fig. 1 shows an example each of a PMC geometry and a PHA cell employing identical fibers of volume fractions $\xi^{\mathrm{I}} = 0.6$ and $\eta^{(\mathrm{I})} = 0.1$, together with the surface mesh employed for a part of the multi-fiber geometry.

The constraint equations required for implementing the periodicity boundary conditions were set up with an in-house program and solutions were obtained with the general-purpose finite element code ABAQUS/Standard (3DS, Dassault Systémes, Providence, RI). The responses to six linearly independent load cases involving uniaxial tension in $x$-, $y$- and $z$-directions as well as simple shear in the $xy$-, $yz$- and $zx$-planes were evaluated by applying appropriate unit loads, so that the stiffness matrix had to be decomposed only once for a given geometry. The resulting macroscopic displacement vectors were used for extracting the macroscopic strains, from which, in turn, the macroscopic elasticity tensor was evaluated. It is worth noting that for the configurations considered here the microscopic stress and strain fields do not vary in the direction of the fibers, i.e., they constitute generalized plane strain states. In principle, such analyses could be done at lower cost with planar models that use special generalized plane strain elements of the type proposed, e.g., by Adams and Crane (1984).

Comparisons of elastic moduli obtained by PMC simulations using different geometrical realizations pertaining to given volume fractions $\xi^{\mathrm{I}}$ and $\eta^{(\mathrm{I})}$ showed relative differences below 1% in most cases. However, for elevated fiber volume fractions and high elastic contrasts these differences exceeded 5% for some configurations. Accordingly, the PMC models must be viewed as being statistical volume elements in the sense of Ostoja-Starzewski (2006) rather than proper representative volume elements. In order to improve this aspect of the models' behavior, $\mathbf{E}^*$ may be evaluated as the ensemble average over the predictions obtained from a number of different, statistically equivalent geometries, compare Kanit et al. (2003). For the present study, four such volume elements were used for each set of volume fractions considered, which positively affected the Zener parameters describing deviations from macroscopic transverse isotropy. Removing the remaining deviations, on the one hand, is in agreement with the "standard assumption" on the macroscopic symmetry of composites reinforced by aligned fibers and, on the other hand, facilitates comparisons with the other models. In order to achieve this, expressions due to Moakher and Norris (2006) were used for finding the transversally isotropic tensor closest to a given ensemble averaged elasticity tensor $\mathbf{E}^*$ in terms of log-Euclidean distances. The tensors resulting from this procedure were treated as the final estimates from numerical homogenization.

For comparison with the analytical models phase averages of the microfields, $\langle f\rangle^{(\mathrm{p})}$, were approximated numerically, volume integrals being replaced by weighted sums of the type

$$\langle f\rangle^{(\mathrm{p})} = \frac{1}{\Omega^{(\mathrm{p})}}\int_{\Omega^{(\mathrm{p})}} f(\mathbf{x})\,d\Omega \approx \frac{1}{\Omega^{(\mathrm{p})}}\sum_{i=1}^{N^{(\mathrm{p})}} f_i\,\Omega_i \quad . \tag{18}$$

Here $f_i$ and $\Omega_i$ are the function value at and the volume of, respectively, the $i$th integration point within a given phase volume $\Omega^{(\mathrm{p})}$ that contains a total of $N^{(\mathrm{p})}$ integration points. In analogy to Böhm (2019) the volumes $\Omega^{(\mathrm{p})}$ were taken to be the union of all appropriate phase volumes from the four volume elements pertaining to a given configuration and, in view of the macroscopic transverse isotropy, all equivalent load cases (e.g., outputs from the two axial shear load cases) were combined. Phase-level standard deviations of the microfields were evaluated from the integration point data by analogy.

Limited convergence tests in terms of the mesh size were carried out. They involved a configuration of fiber volume fraction $\xi^{\mathrm{I}} = 0.7$ and an interphase partial volume fraction of $\eta^{(\mathrm{I})} = 0.5$, i.e., a thick coating. Predictions from five different discretizations using between $1.37\times10^6$ (which corresponds to the mesh as used in Section 3) to $9.25\times10^6$ nodes were compared for material data sets M2 and M3 (compare Table 1). Relative differences in the evaluated effective moduli were found to fall below 0.1% and those in the phase averaged stress components did not exceed 2.5%, with the largest deviations occurring for the transverse stress under transverse normal loading of the high-contrast material data set M2. Differences in the predicted standard deviations of the full-field phase-level stress distributions reached 5.3% for this load case, but differences in the phase-level minima and maxima obtained with the five discretizations remained below 2.5%. This behavior indicates that the element sizes enforced by the specifications for the interphase regions make the numerical results sufficiently independent of mesh size.

### 2.3. Material parameters

Four sets of generic, linear elastic constituent data, M1 to M4, were used in the study, which were primarily selected to cover widely different points in the pertinent parameter space. The Young's modulus of the matrix was set to unity in all cases. Material data sets M1 to M3 employ isotropic constituents, cover a range of elastic contrasts and are identical to the ones employed by Böhm (2019) for composites reinforced by coated particles. For material M1, the stiffness of the coating lies between the ones for matrix and core, whereas for composite M2 the coating is considerably stiffer than the core and markedly stiffer than the matrix. Data set M3 targets interphases that are more compliant than the matrix and markedly more so than the fiber core. The pertinent elastic moduli are listed in Table 1. The fourth material data set, M4, probes the models' behavior when the fibers are transversally isotropic. The interphase in this case was chosen to be somewhat more compliant than the matrix and to be nearly incompressible. The constituents' moduli for material data M4 set are given in Table 2.

Appendix B lists, in tabular form, the elastic moduli of equivalent fibers corresponding to material data sets M2 and M3 obtained with a number of equivalent homogeneous fiber sub-models for selected values of $\eta^{(\mathrm{I})}$.

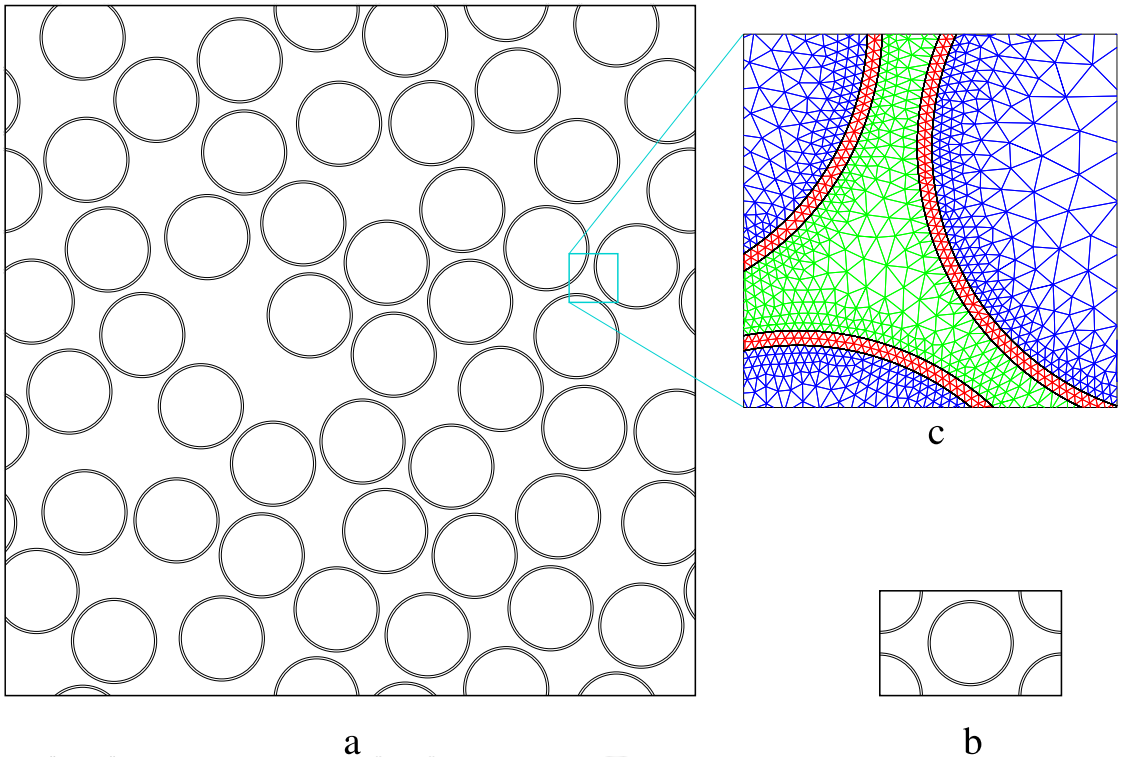


**Fig. 1.** Phase arrangement of a typical multi-fiber volume element (a) and a PHA unit cell (b), both pertaining to volume fractions $\xi^{\mathrm{I}} = 0.6$ and $\eta^{(\mathrm{I})} = 0.1$. (c) shows the surface FE mesh used for a part of the PMC geometry.

**Table 1**
Normalized Young's moduli, $E^{(\mathrm{p})}$, and Poisson numbers, $\nu^{(\mathrm{p})}$, of matrix, core and interphase used for material data sets M1, M2 and M3, respectively.

| mater.set | $E^{(\mathrm{m})}$ | $\nu^{(\mathrm{m})}$ | $E^{(\mathrm{c})}$ | $\nu^{(\mathrm{c})}$ | $E^{(\mathrm{I})}$ | $\nu^{(\mathrm{I})}$ |
|---|---|---|---|---|---|---|
| M1 | 1.0 | 0.33 | 10.0 | 0.1 | 3.0 | 0.2 |
| M2 | 1.0 | 0.33 | 10.0 | 0.1 | 50.0 | 0.2 |
| M3 | 1.0 | 0.33 | 10.0 | 0.1 | 0.2 | 0.2 |

**Table 2**
Normalized axial and transverse Young's moduli, $E_{\mathrm{A}}^{(\mathrm{p})}$ and $E_{\mathrm{T}}^{(\mathrm{p})}$, axial and transverse shear moduli, $G_{\mathrm{A}}^{(\mathrm{p})}$ and $G_{\mathrm{T}}^{(\mathrm{p})}$, axial and transverse Poisson numbers, $\nu_{\mathrm{A}}^{(\mathrm{p})}$ and $\nu_{\mathrm{T}}^{(\mathrm{p})}$, as well as transverse bulk modulus, $K_{\mathrm{T}}^{(\mathrm{p})}$, of matrix, core and interphase layer, respectively, used for material data set M4.

| Phase | $E_{\mathrm{A}}$ | $E_{\mathrm{T}}$ | $G_{\mathrm{A}}$ | $G_{\mathrm{T}}$ | $\nu_{\mathrm{A}}$ | $\nu_{\mathrm{T}}$ | $K_{\mathrm{T}}$ |
|---|---|---|---|---|---|---|---|
| $^{(\mathrm{m})}$ | 1.0 | 1.0 | 0.376 | 0.376 | 0.33 | 0.33 | 1.106 |
| $^{(\mathrm{c})}$ | 20.0 | 2.0 | 2.000 | 0.870 | 0.10 | 0.15 | 1.179 |
| $^{(\mathrm{I})}$ | 0.5 | 0.5 | 0.168 | 0.168 | 0.49 | 0.49 | 8.389 |

## 3. Results and discussion

The analytical procedures for which results are compared can be split into three groups. The first consists of two-step methods that use the exact results for the dilute partial strain concentration tensors of coated cylinders, $\bar{\mathbf{T}}_{\mathrm{dil}}^{(\mathrm{c,m})}$ and $\bar{\mathbf{T}}_{\mathrm{dil}}^{(\mathrm{I,m})}$, provided by Chatzigeorgiou and Meraghni (2019), to evaluate the equivalent tensors $\bar{\mathbf{A}}_{\mathrm{dil,eqv}}^{\mathrm{I}}$ and $\mathbf{E}_{\mathrm{eqv}}^{\mathrm{I}}$ via Eqs. (13) and (15), respectively. This equivalent homogeneous fiber sub-model is combined with composite-level sub-models taking the form of a standard Benveniste-type Mori–Tanaka scheme, see Eq. (A.3), to give model **EMT**, with a Differential Scheme, see Eq. (A.4), to give model **EDS**, with the three-point estimates of Torquato (1998) to give model **E3PE**, and with the Method of Conditional Moments of Khoroshun et al. (1988), see Eqs. (A.5) and (A.6), to give model **EMCM**. The Generalized Self-Consistent scheme of Hervé and Zaoui (1995), via model **EGSC**, also is part of this group. Model E3PE employs the three-point statistical parameters for identical hard cylinders proposed by Torquato and Lado (1992).

The second group of analytical models describe the equivalent inhomogeneities via two-phase Mori–Tanaka-type schemes, compare Eqs. (A.7) and (A.8). Following Friebel et al. (2006) this data is combined with a Mori–Tanaka scheme at the composite level, Eq. (A.3), to obtain a "Mori–Tanaka–Mori–Tanaka" model. Identical predictions were obtained with this method, with the GEEE of Ghazavizadeh et al. (2019) in the simplified form of Eq. (A.8), and with the RDIM model of Dinzart et al. (2016) for all configurations considered. The same responses can also be recovered by using two-phase Maxwell schemes, compare, e.g., Torquato (2002), at both levels. Results from this cluster of methods are marked as **MTMT** in the plots. The hierarchical multi-interphase model of Li et al. (2011) uses the same equivalent elasticity tensors as the MTMT scheme, but employs different equivalent dilute strain concentration tensors, see Eq. (A.9). The predictions marked as **HMM** in the plots were obtained by combining these descriptors with a Mori–Tanaka model at the composite level. Furthermore, as an example of the "construction kit" approach discussed in Section 2.1, a combination of the Mori–Tanaka method at the equivalent homogeneous fiber level with the Differential Scheme at the composite level, referred to as **MTDS**, is considered.

Among the two-step models listed above, the MTDS, to the author's knowledge, is new and the E3PB, E3PE, EDS and EMCM were applied to composites reinforced by continuous, aligned, coated fibers for the first time.

The third group of analytical schemes includes the model of Dunn and Ledbetter (1995), which combines equivalent strain concentration tensors obtained with the DIM of Hori and Nemat-Nasser (1993), compare Eq. (A.10), with Eqs. (12) and (A.3) at the composite level. Its predictions are marked as **DIMM**. In addition, the one-step method of Birman (2021), compare Eq. (A.2), denoted by **BIR**, is covered. Tests were also carried out with the method of Liu and Bian (2019), which, however, gave rise to non-symmetric elasticity tensors for some of the configurations studied here.

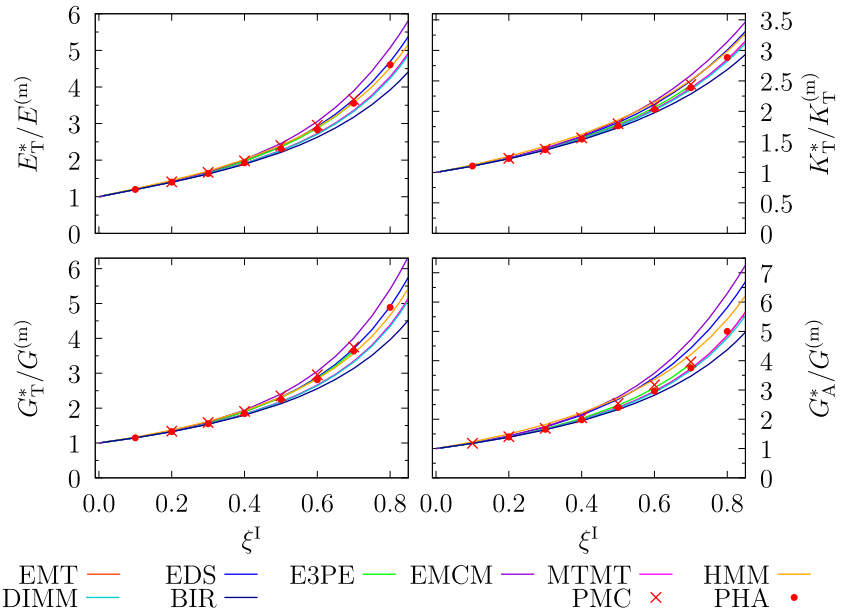


**Fig. 2.** Normalized effective transverse Young's modulus $E_T^*/E^{(m)}$, transverse bulk modulus $K_T^*/K_T^{(m)}$, transverse shear modulus $G_T^*/G^{(m)}$ and axial shear modulus $G_A^*/G^{(m)}$ predicted for composites reinforced by coated continuous fibers. Results are given as functions of the volume fraction of the compound fibers, $\xi^I$. They pertain to an interphase partial volume fraction of $\eta^{(I)} = 0.1$ and to material data set M1.

In order to avoid excessive cluttering of the plots, neither two-phase bounds evaluated with the equivalent fiber data nor three-phase bounds are shown in Figs. 2 to 5. They are, however, provided and discussed in Appendix C.

Numerical results generated with the multi-fiber periodic volume elements are marked as **PMC** and data obtained with periodic hexagonal arrays as **PHA**. PMC predictions were evaluated for inhomogeneity volume fractions of $\xi^I = 0.2$, 0.3, 0.4, 0.5, 0.6 and 0.7 for materials M1, M2 and M3 and for $\xi^I = 0.5$ as well as $\xi^I = 0.7$ in the case of material M4. For each value of $\xi^I$ the partial interphase volume fractions of $\eta^{(I)} = 0.1$, 0.2 and 0.5 were covered, and $\eta^{(I)} = 0.05$ and 0.9 were studied as well for $\xi^I = 0.7$. PHA results were obtained for the same configurations and, in addition, for $\xi^I = 0.1$ as well as $\xi^I = 0.8$. Because the predictions of the various models become increasingly similar as dilute configurations are approached, periodic multi-fiber volume elements were not considered worth the considerable numerical cost for volume fractions below $\xi^I = 0.2$. The upper limit of $\xi^I = 0.7$ for the PMC models is due to limitations of the algorithm used for generating such phase arrangements with the minimum inter-fiber distance specified in Section 2.2.

Among the values of $\eta^{(I)}$ considered here, the higher ones fall outside the range typical of fiber coatings, but were included in order to give a broader picture of the capabilities of the various methods. For brevity the following discussion covers only part of the above data; a more complete set of results is provided in the supplementary material.

### 3.1. Macroscopic responses

Predictions for the effective axial Young's modulus, $E_A^*$, provided by the various methods in most cases differ only marginally from each other (and from the "rules of mixture"). Accordingly, this modulus is not considered further in the present work. In the plots all moduli are normalized with respect to the corresponding modulus of the matrix.

Fig. 2 shows predictions for the normalized transverse Young's modulus, $E_T^*/E^{(m)}$, transverse bulk modulus, $K_T^*/K_T^{(m)}$, transverse shear modulus, $G_T^*/G^{(m)}$ and axial shear modulus, $G_A^*/G^{(m)}$ as functions of the inhomogeneity volume fraction $\xi^I$. The moduli were evaluated for material data set M1 at an interphase partial volume fraction of $\eta^{(I)} = 0.1$. There is not much to choose between the various methods for fiber volume fractions below, say, $\xi^I = 0.25$ but differences between them become obvious at higher values of $\xi^I$ and are most pronounced for the axial and transverse shear moduli.

Among the two-step schemes based on the exact solutions for the dilute equivalent fibers, for material data set M1 the predictions of the Mori–Tanaka model (EMT) for the moduli can be seen to give the lowest effective moduli, followed by those of the three-point estimates (E3PE), the Differential Scheme (EDS) and the Method of Conditional Moments (EMCM). All of these results fulfill the two-phase Hashin–Shtrikman bounds and the latter group complies with the three-point bounds. The EMT, EGSC (not shown in Fig. 2 because its differences to the EMT in $E_T^*$ and $G_T^*$ are too small to be resolved there) and MTMT methods give identical results for the effective moduli $E_A^*$, $G_A^*$ and $K_T^*$ — this behavior was consistently observed for all configurations covered in the present study. Identical predictions for these moduli can also be obtained by recursively applying expressions of the two-phase Composite Cylinder Assemblage (CCA) of Hashin and Rosen (1964), as shown by Hervé and Zaoui (1995) for the case of the Generalized Self-Consistent Scheme. This may indicate a connection of the above two-step approaches to microgeometries with widely dispersed fiber radii (among the analytical models used in this study, only the E3PE and E3PB unequivocally pertain to identical fibers). The MTDS scheme (not shown) closely tracks the EDS results for all effective moduli. The Double Inclusion Model (DIMM) and Birman's method (BIR) predict slightly lower effective moduli than the other analytical methods. The results generated with periodic multi-fiber cells (PMC) for $G_A^*$ and $K_T^*$ straddle the E3PE ones, whereas those for the moduli $E_T^*$ and $G_T^*$ are closer to the EDS curves. The periodic hexagonal arrays (PHA) yield slightly lower values for the effective moduli than the PMC model.

The elastic contrasts between equivalent fibers and matrix for material data set M2 considerably exceed the ones pertaining to material M1, compare Table B.1 for $\eta^{(I)} = 0.1$. As a consequence, differences between the predictions for the effective elastic moduli from the various models are more pronounced, as can be seen for the case of the transverse shear modulus presented in Fig. 3. The two plots in this figure show $G_T^*/G^{(m)}$ for two partial volume fractions of the interphase, $\eta^{(I)} = 0.1$ and $\eta^{(I)} = 0.5$, both of which lead to qualitatively similar, but quantitatively different predictions. The bounds on the effective elastic moduli presented in Fig. C1 pertain to the configuration with $\eta^{(I)} = 0.1$.

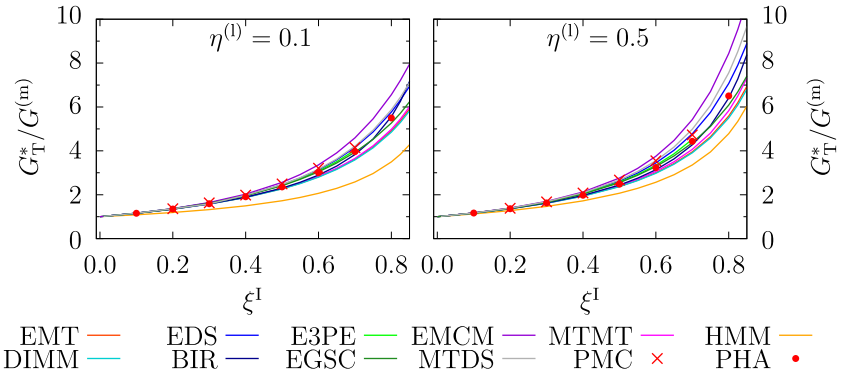


**Fig. 3.** Normalized effective transverse shear modulus $G_\mathrm{T}^*/G^{(\mathrm{m})}$ predicted for composites reinforced by coated continuous fibers. Results are given as functions of the volume fraction of the compound fibers, $\xi^\mathrm{I}$. They pertain to interphase partial volume fractions of $\eta^{(\mathrm{I})} = 0.1$ and $\eta^{(\mathrm{I})} = 0.5$, respectively, and were evaluated for material data set M2.

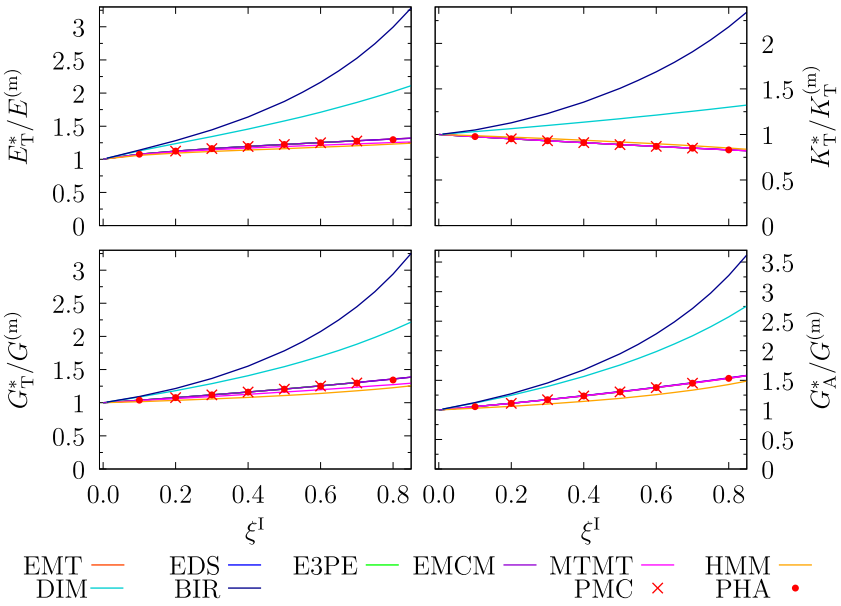


**Fig. 4.** Normalized effective transverse Young's modulus $E_\mathrm{T}^*/E^{(\mathrm{m})}$, transverse bulk modulus $K_\mathrm{T}^*/K_\mathrm{T}^{(\mathrm{m})}$, transverse shear modulus $G_\mathrm{T}^*/G^{(\mathrm{m})}$ and axial shear modulus $G_\mathrm{A}^*/G^{(\mathrm{m})}$ predicted for composites reinforced by coated continuous fibers. Results are given as functions of the volume fraction of the compound fibers, $\xi^\mathrm{I}$. They pertain to an interphase partial volume fraction of $\eta^{(\mathrm{I})} = 0.2$ and to material data set M3.

Compared to Fig. 2 the main difference concerning the analytical models is that the HMM clearly underpredicts $G_\mathrm{T}^*$ for the high-contrast material M2. Also, in Fig. 3 the MTMT-scheme can be seen to yield slightly higher moduli than the EMT, and the predictions of the EGSC are somewhat stiffer again. Furthermore, in this high-contrast situation the MTDS estimates can be seen to be somewhat stiffer than the EDS ones. These differences grow as the thickness of the interphase is increased. Birman's scheme provides reasonable results for fiber volume fractions up to $\xi^\mathrm{I} \approx 0.75$, but starts to "run away" for higher values. The numerical results obtained with multi-fiber volume elements (PMC) agree very well with analytical predictions of the Differential Scheme, well with those of the three-point estimates and fairly well with the self-consistent and Mori–Tanaka data. As in Fig. 2 the PHA geometries provide lower predictions than the PMC ones, with the largest deviations occurring for fiber volume fractions around $\xi^\mathrm{I} \approx 0.6$.

Fig. 4 compares predictions for the effective moduli $E_\mathrm{T}^*$, $K_\mathrm{T}^*$, $G_\mathrm{T}^*$ and $G_\mathrm{A}^*$ obtained for material data set M3 as functions of the volume fraction of the compound fibers, $\xi^\mathrm{I}$. The partial volume fraction of the highly compliant interphase is set to $\eta^{(\mathrm{I})} = 0.2$, leading to elastic contrasts between matrix and equivalent fibers close to unity for the above moduli, see Table B.3. Combined with the marked elastic contrast between fiber core and coating, this tends to challenge the capabilities of the models to correctly predict the stress partitioning between the phases. Whereas the approaches using the exact and the Mori–Tanaka solutions for the equivalent fibers give nearly identical predictions as the numerical models, the DIMM and Birman's method do not pass this test and even fail to capture the decrease of $K_\mathrm{T}^*$ with increasing $\xi^\mathrm{I}$. The HMM shows minor deviations from the numerical predictions. Bounds pertaining to this configuration are given in Fig. C2. At an interphase partial volume fraction $\eta^{(\mathrm{I})} = 0.01$ the elastic contrasts resulting for material M3 clearly exceed unity, compare Table B.2, and at $\eta^{(\mathrm{I})} = 0.5$ all of them fall considerably below this value. Under the former conditions the DIMM does better and the HMM worse compared to $\eta^{(\mathrm{I})} = 0.2$, and vice versa for the thick interphase.

Another aspect of the effective behavior of composites reinforced by unidirectional, coated fibers is explored in Fig. 5, which shows the dependence of the effective moduli $E_\mathrm{T}^*$, $K_\mathrm{T}^*$, $G_\mathrm{T}^*$ and $G_\mathrm{A}^*$ on the partial volume fraction of the interphase, $\eta^{(\mathrm{I})}$, and thus on the interphase thickness. The results were evaluated for material data set M4, i.e., for transversally isotropic fiber cores, at a fixed fiber volume fraction of $\xi^\mathrm{I} = 0.7$. Again, the numerical simulations as well as most analytical models provide similar predictions. However, the results of Birman's model are clearly on the high side for all moduli shown and for coating partial volume fractions between, say, 0.05 and 0.95. This behavior is

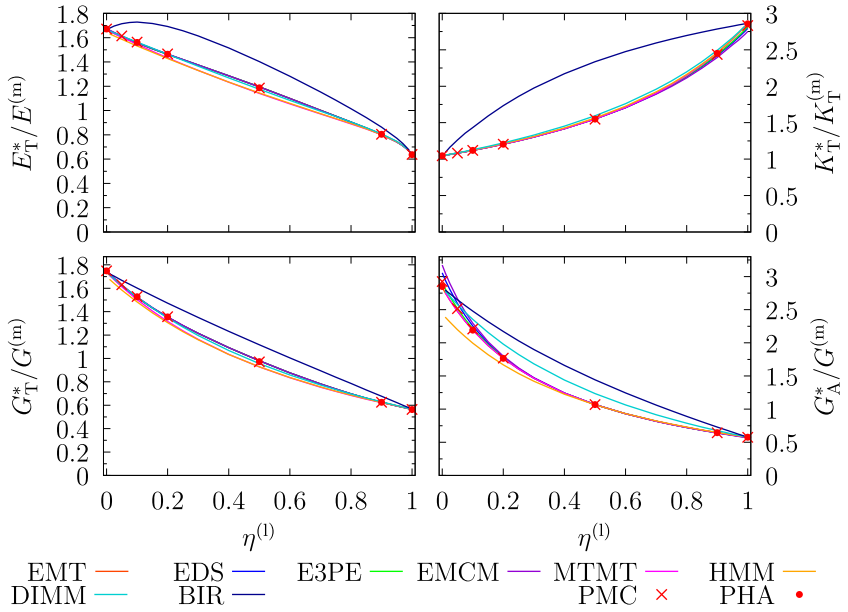


**Fig. 5.** Normalized effective transverse Young's modulus $E_T^*/E^{(m)}$, transverse bulk modulus $K_T^*/K_T^{(m)}$, axial shear modulus $G_A^*/G^{(m)}$ and transverse shear modulus $G_T^*/G^{(m)}$, predicted for composites reinforced by coated continuous fibers. Results are given as functions of the interphase partial volume fraction, $\eta^{(l)}$. They pertain to a volume fraction of the compound fibers of $\xi^I = 0.7$ and to material data set M4.

most marked in the case of the transverse bulk modulus, where the nearly incompressible behavior of the interphase may play a role. For the effective axial shear modulus the DIMM delivers high and the HMM low predictions. The differences evident in the results for $\eta^{(l)} = 0.0$ and $\eta^{(l)} = 1.0$ are due to the fact that these two configurations represent two-phase composites, for which the various composite-level sub-models in general do not give identical predictions. As in Figs. 2 and 4 results for the EGSC and MTDS estimates are not shown because they cannot be distinguished from the results for the EMT and EDS, respectively, in the plots.

Taken together, Figs. 2 to 5 show that the analytical models based on the exact solutions for the dilute, equivalent fibers consistently provide results that match the numerical predictions very well for all configurations and all moduli considered here. The best quantitative agreement with the numerical results was obtained when the three-point estimates, E3PE, and the differential scheme, EDS, were used as composite-level sub-models, with the former tending to provide a closer match at moderate elastic contrasts and the latter at elevated ones. Combining the exact dilute solutions with the Mori–Tanaka and Generalized Self-Consistent schemes also led to consistently good agreement with the numerical results. Among the analytical approaches that treat coated, cylindrical fibers as special cases of coated ellipsoids, the cluster of methods encompassing the MTMT, the GEEE and the RDIM reliably provided predictions that are close to the ones of the EMT. The MTDS model was found to track the EDS fairly well, indicating that this method may be of interest for modeling general coated, spheroidal or ellipsoidal inhomogeneities in high-contrast settings. The favorable behavior of this group of methods is somewhat surprising because Mori–Tanaka approaches were not designed for describing dilute, coated configurations. The other analytical models covered in the present study show considerable weaknesses for one or more of the configurations considered.

Numerical predictions for the effective elastic moduli obtained with periodic hexagonal arrays of fibers were found to deviate systematically, but not markedly from results obtained by periodic homogenization of multi-fiber volume elements.

Finally, it is worth mentioning that the modeling schemes giving favorable results for the effective elastic responses also showed similar qualities in estimating the macroscopic thermal expansion behavior. It may also be expected that among the analytical schemes the ones making use of the exact solutions for the dilute equivalent fibers will be most suitable for studying composites with nonlinear matrix behavior.

### 3.2. Microscopic responses

The numerical methods and many of the analytical approaches used in the present work allow evaluating phase averaged strain and stress fields. In this section selected results of the latter type are compared for the unit transverse normal and shear load cases employed for building up the effective elastic tensors. Phase averages and standard deviations of stress components were evaluated from model PMC by Eq. (18); the latter are visualized via error bars in Figs. 6 and 7. In interpreting these standard deviations it should be kept in mind that the above load cases imply marked circumferential variations of the stress tensors in and around fibers.

Predictions for the phase averaged transverse normal stresses are shown in Fig. 6 for material data set M2, i.e., for a stiff interphase, in dependence on the volume fraction of the compound fibers, $\xi^I$. The load case is macroscopic transverse normal loading and the interphase partial volume fraction is set to $\eta^{(l)} = 0.1$. Results are provided for the fiber core, the coating and the matrix, the pertinent phase averaged stress components being denoted as $\langle\sigma_{tr}\rangle^{(c)}$, $\langle\sigma_{tr}\rangle^{(l)}$ and $\langle\sigma_{tr}\rangle^{(m)}$, respectively, and for the average transverse stress in the equivalent inhomogeneity, $\langle\sigma_{tr}\rangle^I$. All analytical two-step schemes using the exact solutions for the equivalent fibers give rise to similar responses which are in good agreement with the numerical predictions. The stresses predicted by the MTMT are also very close to the above results for matrix and equivalent fibers and close for fiber cores and interphases. The HMM, however, yields markedly different results and the DIMM can be seen to clearly underpredict the stresses in the coating layer and to overpredict those in the fiber core to a lesser extent. It is interesting to note that, with the exception of the HMM, the results of all analytical models are much more tightly bunched for the equivalent fibers than for core and interphase. The fluctuations of the stress fields predicted by the multi-fiber full-field model, PMC, can be seen to be considerable in all constituents and especially marked in the interphase for this load case. The rather low value of the standard deviations of $\langle\sigma_{tr}\rangle^{(l)}$

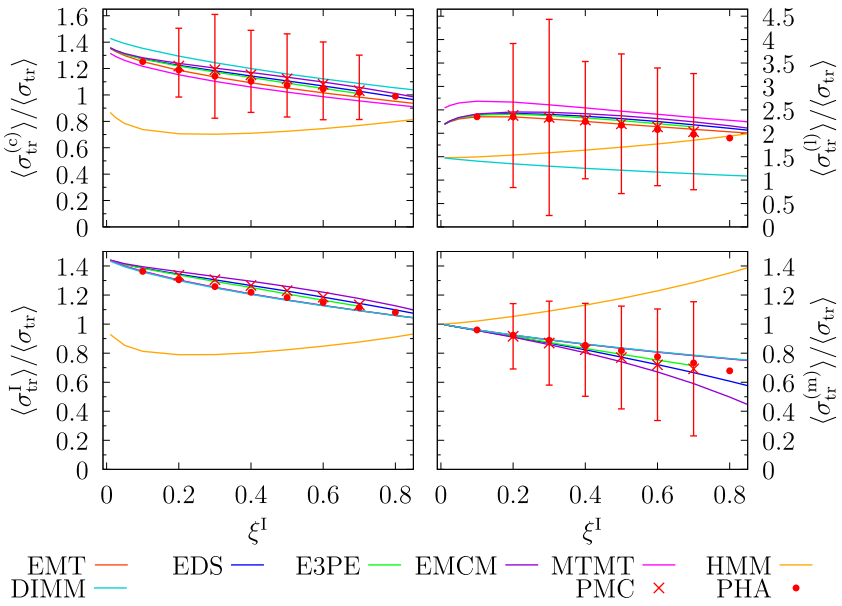


**Fig. 6.** Normalized, phase averaged, transverse normal stresses in the fiber core, the coating, the equivalent fibers and the matrix, $\langle\sigma_{tr}\rangle^{(c)}$, $\langle\sigma_{tr}\rangle^{(l)}$, $\langle\sigma_{tr}\rangle^{I}$ and $\langle\sigma_{tr}\rangle^{(m)}$, respectively, predicted for composites reinforced by coated continuous fibers and loaded by a macroscopic uniaxial transverse stress $\langle\sigma_{tr}\rangle$. Results are given as functions of the volume fraction of the compound fibers, $\xi^I$. They pertain to an interphase partial volume fraction of $\eta^{(l)} = 0.1$ and to material data set M2.

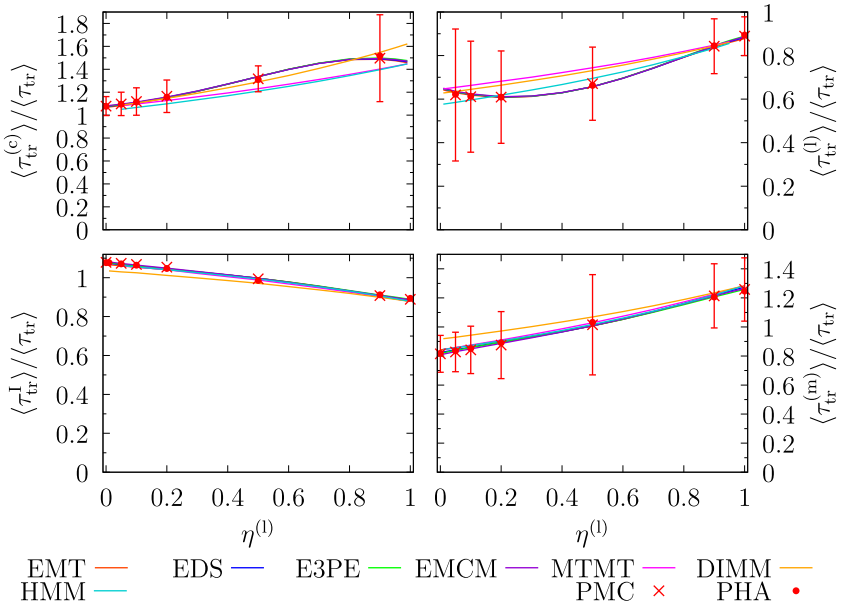


**Fig. 7.** Normalized, phase averaged, transverse shear stresses in the fiber core, the coating, the equivalent fibers and the matrix, $\langle\tau_{tr}\rangle^{(c)}$, $\langle\tau_{tr}\rangle^{(l)}$, $\langle\tau_{tr}\rangle^{I}$ and $\langle\tau_{tr}\rangle^{(m)}$, respectively, predicted for composites reinforced by coated continuous fibers and loaded by a macroscopic transverse shear stress $\langle\tau_{tr}\rangle$. Results are given as functions of the partial volume fraction of the interphase, $\eta^{(l)}$. They pertain to a volume fraction of the compound fibers of $\xi^I = 0.7$ and to material data set M4.

at $\xi^I = 0.4$ may indicate that the number and/or size of the volume elements in the ensemble average is insufficient for fully resolving the pertinent phase-level stress distributions.

Fig. 7 displays predictions for the phase averaged transverse shear stresses due to macroscopic transverse shear loading as functions of the partial volume fraction of the coating, $\eta^{(l)}$. The volume fraction of the compound fibers is set to $\xi^I = 0.7$ and material data set M4 is used, i.e., the same configurations are studied as in Fig. 5. The predictions for the transverse shear stress components in the equivalent fibers, $\langle\tau_{tr}\rangle^{I}$, and the matrix, $\langle\tau_{tr}\rangle^{(m)}$, obtained from the various models are in good agreement for this load case and configuration, only the HMM showing minor deviations. For the phase averages of the transverse shear stresses in the fiber core and the coating, $\langle\tau_{tr}\rangle^{(c)}$ and $\langle\tau_{tr}\rangle^{(l)}$, however, only the two-step schemes based on the rigorous solutions for the equivalent fibers show the same qualitative behavior as the numerical predictions. Interestingly, the MTMT-type estimates differ in this respect.

As in the case of the effective moduli, good agreement in terms of the phase averaged stresses was found between, on the one hand, the analytical approaches based on the exact solutions for the equivalent fibers and, on the other hand, the numerical simulations, with the EDS and E3PE models again doing very well. In the supplementary material a range of results on the "direct" stress responses, i.e., the phase averages of the stress component $\langle\sigma_{ij}\rangle^{(p)}$ due to a macroscopic unit load $\langle\sigma_{ij}\rangle$, are presented for the load cases of uniaxial axial tension, uniaxial transverse tension, axial shear and transverse shear. Clear

differences between the different groups of models are evident; they are especially marked, on the one hand, for the transverse tension and shear load cases and, on the other hand, for applied axial shear. Finally, it should be noted that the local minima and maxima of the full-field stresses as evaluated by the PMC models in many cases differ markedly from the corresponding phase averages.

## 4. Conclusions

Predictions from a number of analytical and numerical modeling schemes for the macroscopic and microscopic elastic responses of composites reinforced by unidirectional, continuous fibers that are coated by a uniform, coaxial interphase layer were compared by studying four generic material data sets. The analytical methods form three groups, viz., two-step schemes based on rigorous solutions for the equivalent fibers, two-step models using Mori–Tanaka-type expressions at the coated-inhomogeneity level, and other descriptions. The numerical models combine Finite-Element-based periodic homogenization with periodic hexagonal or random fiber arrangements.

Analytical models using the exact solutions for the dilute, coated fibers were found to match the numerical simulations very well for all configurations considered, three-point estimates and differential schemes giving especially satisfactory results. Accordingly, this group of methods may be viewed as the most suitable analytical models for composites reinforced by coated fibers. Among the analytical approaches capable of handling coated ellipsoidal inhomogeneities, two-step schemes using Mori–Tanaka-type methods at the coated fiber level acquitted themselves well for the geometries and material parameters considered.

## Funding

This research did not receive any specific grant from funding agencies in the public, commercial, or not-for-profit sectors.

## Declaration of competing interest

The authors declare that they have no known competing financial interests or personal relationships that could have appeared to influence the work reported in this paper.

## Data availability

Data will be made available on request.

## Appendix A. Expressions for some analytical models

This appendix provides expressions for the equivalent strain concentration tensors and/or equivalent elasticity tensors as well as the effective elasticity tensors pertaining to some of the analytical micromechanical models used in the present study. For details and derivations the reader is referred to the original papers. Only approaches that allow writing the above tensors compactly in intrinsic notation are covered.

Many of the relevant methods make use of the dilute partial strain concentration tensor of a uniform, ellipsoidal inhomogeneity $^{(p)}$ embedded in a phase $^{(q)}$, which can be expressed as

$$\bar{\mathbf{T}}^{(p,q)}_{dil} = \left[\mathbf{I} + \mathbf{S}^{(p,q)}\mathbf{C}^{(q)}(\mathbf{E}^{(p)} - \mathbf{E}^{(q)})\right]^{-1} \quad , \tag{A.1}$$

of which Eq. (14) is a special case.

*One-step models*

The approach proposed by Birman (2021) approximates the effective elasticity tensor of a composite reinforced by coated inhomogeneities as

$$\mathbf{E}^{*}_{B} = \mathbf{E}_{cm}(\xi^{(c)}) + \mathbf{E}_{lm}(\xi^{(i)}) - \mathbf{E}_{lm}(\xi^{(c)}) \quad , \tag{A.2}$$

where

$$\begin{aligned}\mathbf{E}_{pm}(\xi^{(q)}) &= \mathbf{E}^{(m)} + \xi^{(q)}(\mathbf{E}^{(p)} - \mathbf{E}^{(m)})\,\bar{\mathbf{T}}^{(p,m)}(\xi^{(q)})\\ \bar{\mathbf{T}}^{(p,m)}(\xi^{(q)}) &= \bar{\mathbf{T}}^{(p,m)}_{dil}\left[(1-\xi^{(q)})\mathbf{I} + \xi^{(q)}\bar{\mathbf{T}}^{(p,m)}_{dil}\right]^{-1} \quad .\end{aligned}$$

are Mori–Tanaka-type expressions and the $\bar{\mathbf{T}}^{(p,m)}_{dil}$ are given by Eq. (A.1).

*Composite-level sub-models*

The three-point estimates (Torquato, 1998) are formulated in terms of elastic moduli and thus are not given here.

Following Benveniste (1987) the Mori–Tanaka non-dilute strain concentration tensor pertaining to an equivalent inhomogeneity, $\bar{\mathbf{A}}^{I}_{MT}$, can be expressed as

$$\bar{\mathbf{A}}^{I}_{MT} = \bar{\mathbf{A}}^{I}_{dil,eqv}\left[\xi^{(m)}\mathbf{I} + \xi^{I}\bar{\mathbf{A}}^{I}_{dil,eqv}\right]^{-1} \tag{A.3}$$

in terms of the dilute equivalent strain concentration tensor, $\bar{\mathbf{A}}^{I}_{dil,eqv}$.

When using the Differential Scheme, see, e.g., Hashin (1988), the effective elasticity tensor is found by integrating up the system of ordinary differential equations

$$\frac{d\mathbf{E}^{*}_{D}}{d\xi^{I}} = \frac{1}{1-\xi^{I}}(\mathbf{E}^{I}_{eqv} - \mathbf{E}^{*}_{D})\bar{\mathbf{T}}^{I,*}_{dil,eqv} \quad , \tag{A.4}$$

which can be done numerically, e.g., by Runge–Kutta methods.

In the Method of Conditional Moments (MCM), the effective elasticity tensor takes the form

$$\begin{aligned}\mathbf{E}^{*}_{MCM} = {}& \xi^{(m)}\mathbf{E}^{(m)} + \xi^{I}\mathbf{E}^{I}_{eqv} - \xi^{I}\xi^{(m)}(\mathbf{E}^{I}_{eqv} - \mathbf{E}^{(m)}) \times\\ & \left[\mathbf{I} + \mathbf{L}^{I,0}\left(\xi^{(m)}\mathbf{E}^{I}_{eqv} + \xi^{I}\mathbf{E}^{(m)} - \mathbf{E}^{(0)}\right)\right]^{-1}\mathbf{L}^{I,0}(\mathbf{E}^{I}_{eqv} - \mathbf{E}^{(m)}) \quad ,\end{aligned} \tag{A.5}$$

see, e.g., Khoroshun et al. (1988) or Nazarenko et al. (2017). Here $\mathbf{L}^{I,0}$ provides information on the two-point statistics of the phase arrangement. Since no expression for this tensor appears to be available for composites reinforced by aligned, continuous fibers, it was approximated for the present study by the Hill tensor of the equivalent inhomogeneity evaluated with respect to the reference material $^{(0)}$, i.e., $\mathbf{L}^{I,0} \approx \mathbf{P}^{I,0} = \mathbf{S}^{I,0}\mathbf{C}^{(0)}$. The reference material was chosen as one of the Hill (1952) bounds,

$$\mathbf{E}^{(0)} = \begin{cases} \xi^{I}\mathbf{E}^{I}_{eqv} + \xi^{(m)}\mathbf{E}^{(m)} & \text{for } \mathbf{E}^{I}_{eqv} \le \mathbf{E}^{(m)} \\ \left[\xi^{I}\mathbf{C}^{I}_{eqv} + \xi^{(m)}\mathbf{C}^{(m)}\right]^{-1} & \text{otherwise} \end{cases} \quad . \tag{A.6}$$

as proposed by Khoroshun et al. (1988).

A dilute composite-level sub-model can be generated by inserting the dilute strain concentration tensors for core and coating together with the corresponding relation $\bar{\mathbf{A}}^{(m)} = \frac{1}{1-\xi^{I}}(\mathbf{I} - \xi^{(c)}\bar{\mathbf{A}}^{(c)}_{dil} - \xi^{(l)}\bar{\mathbf{A}}^{(l)}_{dil})$ into Eq. (7). There is no well-defined, physics-based threshold in terms of $\xi^{I}$ beyond which such models become invalid — as the inhomogeneity volume fraction increases from zero, their predictions deviate more and more from solutions accounting for the interactions between inhomogeneities; the detailed behavior depends on the elastic contrast between the phases. Arrangement effects, including influences of the relative sizes of the inhomogeneities, tend to become smaller as the inhomogeneity volume fraction is decreased. Due to their limitations in handling elevated fiber volume fractions dilute models are not used in the present contribution.

It is also worth mentioning that there is no inherent sensitivity to the absolute size of inhomogeneities in the linear local elasticity models considered in this work.

*Equivalent homogeneous fiber sub-models*

Among the equivalent homogeneous fiber sub-models used in the present work, the rigorous solutions for coated cylinders embedded in an infinite matrix given by Wang et al. (2016) and Chatzigeorgiou and Meraghni (2019) are obtained by solving systems of linear equations to extract the coefficients of displacement ansatz functions for the Navier equations. On this basis dilute, partial strain concentration factors can be evaluated, which allow assembling the dilute, partial strain concentration tensors of core and interphase, $\bar{\mathbf{T}}^{(c,m)}_{dil}$ and $\bar{\mathbf{T}}^{(l,m)}_{dil}$. Because these coincide with the dilute strain concentration tensors, $\bar{\mathbf{A}}^{(c)}_{dil}$ and $\bar{\mathbf{A}}^{(l)}_{dil}$, respectively, Eqs. (11) and (15) can be used to evaluate $\bar{\mathbf{A}}^{I}_{dil,eqv}$ and $\mathbf{E}^{I}_{eqv}$.

A Mori–Tanaka approximation for the elasticity tensor of the equivalent uniform inhomogeneity can be given as

$$\mathbf{E}^{I}_{eqv,MT} = \mathbf{E}^{(l)} + \eta^{(c)}(\mathbf{E}^{(c)} - \mathbf{E}^{(l)})\,\bar{\mathbf{T}}^{(c,l)}_{dil}\left(\eta^{(l)}\mathbf{I} + \eta^{(c)}\bar{\mathbf{T}}^{(c,l)}_{dil}\right)^{-1} \quad , \tag{A.7}$$

where $\bar{\mathbf{T}}^{(c,l)}_{dil}$ is obtained via Eq. (A.1). This may be inserted into Eq. (14) to find the equivalent strain concentration tensor $\bar{\mathbf{A}}^{I}_{dil,eqv,MT}$.

For the case of unidirectional fibers coated by a uniform, coaxial interphase the General Explicit Eshelby-type Estimator of Ghazavizadeh et al. (2019) for the equivalent elasticity tensor reduces to

$$\mathbf{E}^{I}_{eqv,GE} = \mathbf{E}^{(l)} + \eta^{(c)}\left[(\mathbf{E}^{(c)} - \mathbf{E}^{(l)})^{-1} + \eta^{(l)}\mathbf{P}^{(c,l)}\right]^{-1} \tag{A.8}$$

where $\mathbf{P}^{(c,l)} = \mathbf{S}^{(c,l)}\mathbf{C}^{(l)}$ is a Hill tensor. This expression can be shown to be identical to $\mathbf{E}^{I}_{eqv,MT}$ as given in Eq. (A.7). The GEEE is formulated such that no dilute equivalent concentration tensors are required for homogenization.

In the HMM model of Li et al. (2011) the elasticity and strain concentration tensors of the equivalent uniform inhomogeneity are approximated as

$$\begin{aligned}\mathbf{E}^{I}_{eqv,HM} &= \left(\eta^{(c)}\mathbf{E}^{(c)}\bar{\mathbf{T}}^{(c,l)}_{dil} + \eta^{(l)}\mathbf{E}^{(l)}\right)\bar{\mathbf{T}}^{(l,m)}_{dil}\;[\bar{\mathbf{A}}^{I}_{dil,eq,HM}]^{-1}\\ \bar{\mathbf{A}}^{I}_{dil,eqv,HM} &= (\eta^{(c)}\bar{\mathbf{T}}^{(c,l)}_{dil} + \eta^{(l)}\mathbf{I})\,\bar{\mathbf{T}}^{(l,m)}_{dil} \quad .\end{aligned} \tag{A.9}$$

Whereas $\mathbf{E}^{I}_{eqv,HM}$ coincides with the Mori–Tanaka result, Eq. (A.7), $\bar{\mathbf{A}}^{I}_{dil,eqv,HM}$ in general is not compatible with Eq. (14).

The Double Inclusion Method of Hori and Nemat-Nasser (1993) allows approximating the equivalent, dilute strain concentration tensor of a coaxially coated fiber as

$$\begin{aligned}\bar{\mathbf{A}}^{(c)}_{dil,DI} &= \mathbf{I} + \mathbf{S}^{I,m}\mathbf{C}^{(m)}(\mathbf{E}^{(c)} - \mathbf{E}^{(m)})\,\bar{\mathbf{T}}^{(c,m)}_{dil}\\ \bar{\mathbf{A}}^{(l)}_{dil,DI} &= \mathbf{I} + \mathbf{S}^{I,m}\mathbf{C}^{(m)}(\mathbf{E}^{(l)} - \mathbf{E}^{(m)})\,\bar{\mathbf{T}}^{(l,m)}_{dil} \quad ,\end{aligned} \tag{A.10}$$

where the matrix is used as the reference material. $\bar{\mathbf{A}}^{I}_{dil,eqv,DI}$ can then be evaluated via Eq. (13) or (14).

## Appendix B. Elastic moduli of equivalent inhomogeneities

When following the "construction kit" approach discussed in Section 2.1 an assessment of the capabilities of the individual sub-models is of interest. Whereas the behavior of the composite-level sub-models is well covered in the literature, fewer results are available on the equivalent homogeneous fiber sub-models. Due to the phase geometries, the equivalent fibers show transversally isotropic symmetry even if both the fiber core and the coating layer are isotropic.

Table B.1 compares predictions for the elastic contrasts (elastic moduli normalized with respect to the corresponding matrix properties) of the equivalent continuous fibers for data set M2, compare Table 1, and an interphase partial volume fraction of $\eta^{(l)} = 0.1$. Tables B.2 and B.3 provide analogous results for data set M3 at $\eta^{(l)} = 0.01$ and $\eta^{(l)} = 0.2$, respectively. The exact results obtained from the dilute concentration tensors given by Chatzigeorgiou and Meraghni (2019) via Eqs. (13) and (15), the Mori–Tanaka approximations (MTM) evaluated from Eq. (A.7), the predictions of the Differential Scheme (DS) obtained from an analog to Eq. (A.4) as well as the DIM approximations evaluated via Eqs. (15) and (A.10) are given in each case. The results marked as MTM also pertain to the GEEE, RDIM and HMM models.

**Table B.1**
Normalized axial and transverse Young's moduli, axial and transverse shear moduli as well as transverse bulk modulus of the equivalent fibers evaluated by different models for material data set M2 and an interphase partial volume fraction of $\eta^{(l)} = 0.1$.

| Model | $E^{I}_{A,eqv}/E^{(m)}$ | $E^{I}_{T,eqv}/E^{(m)}$ | $G^{I}_{A,eqv}/G^{(m)}$ | $G^{I}_{T,eqv}/G^{(m)}$ | $K^{I}_{T,eqv}/K^{(m)}_{T}$ |
|---|---|---|---|---|---|
| exact | 14.039 | 11.784 | 14.837 | 13.638 | 6.461 |
| MTM | 14.039 | 12.063 | 14.837 | 14.209 | 6.461 |
| DS | 14.025 | 11.572 | 14.291 | 13.728 | 6.117 |
| DIM | 14.001 | 10.921 | 13.180 | 13.154 | 5.633 |

**Table B.2**
Normalized axial and transverse Young's moduli, axial and transverse shear moduli as well as transverse bulk modulus of the equivalent fibers evaluated by different models for material data set M3 and an interphase partial volume fraction of $\eta^{(l)} = 0.01$.

| Model | $E^{I}_{A,eqv}/E^{(m)}$ | $E^{I}_{T,eqv}/E^{(m)}$ | $G^{I}_{A,eqv}/G^{(m)}$ | $G^{I}_{T,eqv}/G^{(m)}$ | $K^{I}_{T,eqv}/K^{(m)}_{T}$ |
|---|---|---|---|---|---|
| exact | 9.902 | 7.608 | 9.491 | 8.838 | 4.098 |
| MTM | 9.902 | 7.594 | 9.491 | 8.810 | 4.098 |
| DS | 9.902 | 8.817 | 11.246 | 10.416 | 4.656 |
| DIM | 9.020 | 8.807 | 10.932 | 10.482 | 4.606 |

**Table B.3**
Normalized axial and transverse Young's moduli, axial and transverse shear moduli as well as transverse bulk modulus of the equivalent fibers evaluated by different models for material data set M3 and an interphase partial volume fraction of $\eta^{(l)} = 0.2$.

| Model | $E^{I}_{A,eqv}/E^{(m)}$ | $E^{I}_{T,eqv}/E^{(m)}$ | $G^{I}_{A,eqv}/G^{(m)}$ | $G^{I}_{T,eqv}/G^{(m)}$ | $K^{I}_{T,eqv}/K^{(m)}_{T}$ |
|---|---|---|---|---|---|
| exact | 8.040 | 1.357 | 1.716 | 1.474 | 0.795 |
| MTM | 8.040 | 1.289 | 1.716 | 1.357 | 0.795 |
| DS | 8.041 | 1.795 | 3.148 | 2.653 | 1.117 |
| DIM | 8.041 | 2.416 | 3.448 | 1.882 | 1.397 |

The stiff coating and fiber core in material data set M2 cause all elastic contrasts between the equivalent fibers and the matrix to markedly exceed unity in Table B.1. In contrast the very thin, highly compliant interphase surrounding a stiff fiber core (material data set M3) covered in Table B.2 gives rise to small reductions in the equivalent moduli compared to those of the core. If the compliant coating layer of material M3 is thicker at $\eta^{(l)} = 0.2$, the elastic contrasts are close to unity for all equivalent moduli except $E^{I}_{A,eqv}$, see Table B.3, and for a very thick interface, $\eta^{(l)} = 0.5$, they fall clearly below unity. In the latter cases, the considerable elastic contrasts between core and coating in material data set M3, e.g. $E^{(c)}/E^{(l)} = 50$, accentuate the differences between the predictions of the different equivalent homogeneous fiber sub-models. The value of $\eta^{(l)}$ at which a modulus becomes identical for matrix and equivalent fiber for a material like M3 depends on the modulus considered, implying that a simply coated inhomogeneity that is strictly neutral in the transverse plane does not exist in general.

The equivalent moduli $E^{I}_{A}$, $G^{I}_{A}$ and $K^{I}_{T}$ predicted when using the MTM as the equivalent homogeneous fiber sub-model can be seen to coincide with the exact results in the above three cases, and the differences in $E^{I}_{T}$ and $G^{I}_{T}$ remain rather small. The predictions obtained with the DIM, however, clearly deviate from the exact solutions for all equivalent moduli, the differences being pronounced for the thick compliant coating, Table B.3. In the latter case the DS, too, deviates clearly from the exact results, making the MTM a better choice for a general-purpose equivalent homogeneous fiber sub-model. The differences between the predictions of the models vanish in the limit of very thin interphases.

## Appendix C. Bounds on effective moduli

Figs. C1 and C2 present results obtained with bounding schemes. The three-phase Hashin–Shtrikman–Willis bounds (Willis, 1977) are marked as **HSW**. The two sets of two-phase bounds, viz., the Hashin–Shtrikman-bounds, **EHS**, as well as the three-point bounds, **E3PB**, are

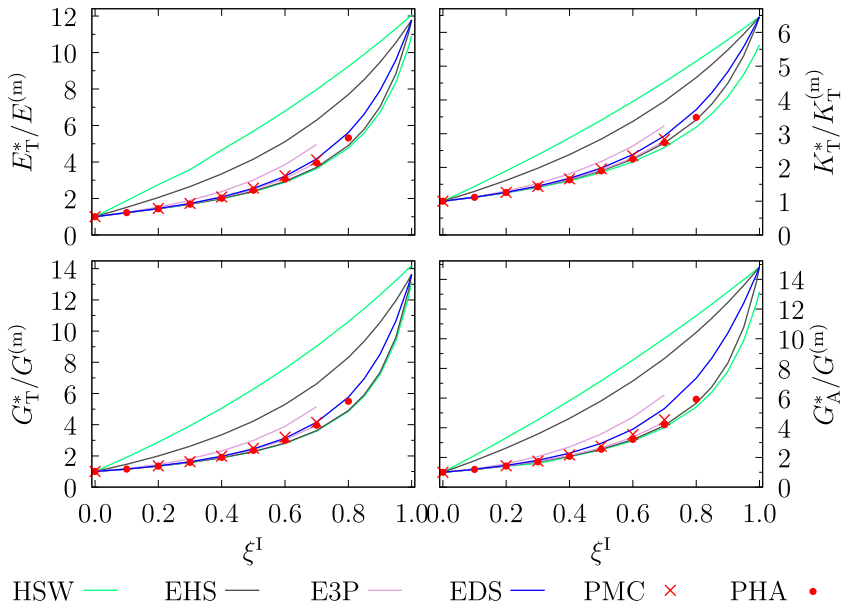


**Fig. C1.** Bounds on and estimates for the normalized effective transverse Young's modulus $E_T^*/E^{(m)}$, transverse bulk modulus $K_T^*/K_T^{(m)}$, transverse shear modulus $G_T^*/G^{(m)}$ and axial shear modulus $G_A^*/G^{(m)}$, respectively, predicted for composites reinforced by coated continuous fibers. Results are given as functions of the volume fraction of the compound fibers, $\xi^I$. They pertain to an interphase partial volume fraction of $\eta^{(I)} = 0.1$ and to material data set M2.

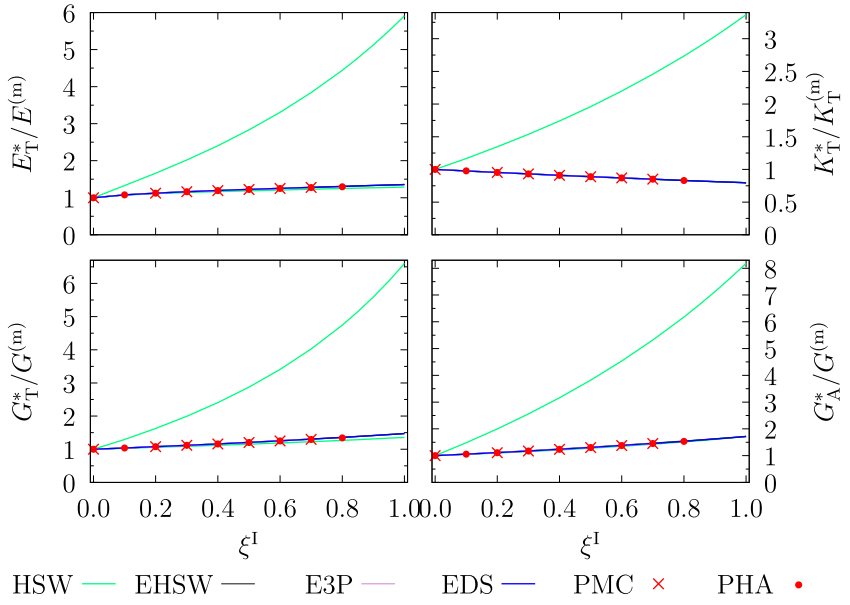


**Fig. C2.** Bounds on and estimates for the normalized effective transverse Young's modulus $E_T^*/E^{(m)}$, transverse bulk modulus $K_T^*/K_T^{(m)}$, transverse shear modulus $G_T^*/G^{(m)}$ and axial shear modulus $G_A^*/G^{(m)}$, respectively, predicted for composites reinforced by coated continuous fibers. Results are given as functions of the volume fraction of the compound fibers, $\xi^I$. They pertain to an interphase partial volume fraction of $\eta^{(I)} = 0.2$ and to material data set M3.

based on equivalent fibers described via the exact results of Chatzigeorgiou and Meraghni (2019). In cases where the moduli of equivalent fibers and matrix were not well ordered (M3, $\eta^{(I)} = 0.2$ and $\eta^{(I)} = 0.5$, as well as M4, $\eta^{(I)} = 0.5$) two-phase Hashin–Shtrikman–Willis bounds, marked as **EHSW**, employing synthetic reference materials were used instead of the classical Hashin–Shtrikman bounds; for all other configurations the EHS and EHSW bounds coincide. In addition, results of the Differential Scheme (EDS) and numerical predictions from multi-fiber volume elements (PMC) as well as periodic hexagonal arrays of fibers (PHA) are shown for the normalized effective transverse Young's modulus, transverse bulk modulus, transverse shear modulus and axial shear modulus.

In Fig. C1, which pertains to an interphase partial volume fraction of $\eta^{(I)} = 0.1$ and material data set M2, the bounds can be seen to form a clear hierarchy, with the two-phase three-point bounds, E3PB, falling within the two-phase Hashin–Shtrikman bounds, EHS, which comply with the three-phase Hashin–Shtrikman–Willis bounds, HSW (which, in turn, lie within the Hill (1952) bounds not shown here). Both the EDS and the PMC results fulfill all three sets of bounds, whereas the PHA predictions typically fall below the two-phase E3PB lower bounds. Analogous behavior was found for all configurations considered in the present work.

Because for material data set M2 the equivalent fibers are considerably stiffer than the matrix, compare Table B.1, the EDS and the numerical estimates closely approach the lower bounds and the EHS lower bounds coincide with the predictions of the EMT. The differences between the lower three-phase and two-phase bounds are small, whereas those between the upper bounds are more pronounced,

the two-phase Hashin–Shtrikman bounds being clearly tighter than the three-phase ones. Similar behavior was obtained for material M1. From a physical point of view the behavior shown in Fig. C1 reflects the differences in the two-point probability distributions pertaining to three-phase geometries involving aligned, coated fibers vs. two "independent" aligned inhomogeneity phases. The HSW upper bounds pertain to the latter type of configuration, which is geometrically much less constrained than coated arrangements, making these bounds slacker.

For material M3 and an interphase partial volume fraction of $\eta^{(\mathrm{I})} = 0.2$ the elastic contrasts $E_{\mathrm{T}}^{\mathrm{I}}/E_{\mathrm{T}}^{(\mathrm{m})}$, $K_{\mathrm{T}}^{\mathrm{I}}/K_{\mathrm{T}}^{(\mathrm{m})}$, $G_{\mathrm{T}}^{\mathrm{I}}/G_{\mathrm{T}}^{(\mathrm{m})}$ and $G_{\mathrm{A}}^{\mathrm{I}}/G_{\mathrm{A}}^{(\mathrm{m})}$ are fairly close to unity, compare Table B.3. As a consequence, the two-phase bounds as well as the EDS, PMC and PHA estimates nearly coincide. This behavior is evident in Fig. C2 (which pertains to the same configuration as Fig. 4). The estimates and the two-phase bounds remain close to, but slightly above the lower three-phase Hashin–Shtrikman–Willis bounds; the upper three-phase bounds, however, can be seen to be markedly higher. The marked slackness of the three-phase bounds for this configuration evident in Fig. C2 is due to the pronounced difference in the moduli of the stiffest and most compliant constituents in material data set M3, which largely determine the properties of the lower and upper reference media. Thus, in this case the stronger geometrical constraint underlying the two-phase bounds based on equivalent fibers has rather extreme consequences. It may be noted that all results given in Fig. 4 fall within the three-phase bounds of Fig. C2.

The majority of numerical results obtained with PMC models in this study comply with the three-point bounds, with a few minor deviations occurring for material data sets M3 and M4, where the bounds may be extremely tight. Similarly, the PHA predictions largely comply with the Hashin–Shtrikman-type bounds. An analogous behavior was also observed with respect to the numerical predictions for $G_{\mathrm{T}}^{*}$ when comparing with the intervals recently proposed for this effective modulus by Firooz et al. (2019) with the moduli of the equivalent fibers.

## Appendix D. Supplementary data

Supplementary material related to this article can be found online at https://doi.org/10.1016/j.ijsolstr.2022.112093.

## References


Aboutajeddine, A., Neale, K., 2005. The double-inclusion model: A new formulation and new estimates. Mech. Mater. 37, 331–341. http://dx.doi.org/10.1016/j.mechmat.2003.08.016.

Achenbach, J., Zhu, H., 1990. Effect of interphases on micro and macromechanical behavior of hexagonal-array fiber composites. J. Appl. Mech. 57, 956–963. http://dx.doi.org/10.1115/1.2897667.

Adams, D., 1987. A micromechanics analysis of the influence of the interface on the performance of polymer-matrix composites. J. Reinf. Plast. Compos. 6, 66–88. http://dx.doi.org/10.1177/073168448700600106.

Adams, D., Crane, D., 1984. Finite element micromechanical analysis of a unidirectional composite including longitudinal shear loading. Comput. Struct. 18, 1153–1165. http://dx.doi.org/10.1016/0045-7949(84)90160-3.

Asp, L., Greenhalgh, E., 2014. Structural power composites. Compos. Sci. Technol. 101, 41–61. http://dx.doi.org/10.1016/j.compscitech.2014.06.020.

Benveniste, Y., 1987. A new approach to the application of Mori–Tanaka's theory in composite materials. Mech. Mater. 6, 147–157. http://dx.doi.org/10.1016/0167-6636(87)90005-6.

Benveniste, Y., Dvorak, G., Chen, T., 1989. Stress fields in composites with coated inclusions. Mech. Mater. 7, 305–317. http://dx.doi.org/10.1016/0167-6636(89)90021-5.

Berbenni, S., Cherkaoui, M., 2010. Homogenization of multicoated inclusion–reinforced linear elastic composites with eigenstrains: Application to thermoelastic behavior. Phil. Mag. 90, 3003–3026. http://dx.doi.org/10.1080/14786431003767033.

Birman, V., 2021. Stiffness of composites with coated inclusions. Compos. Commun. 24, 100604. http://dx.doi.org/10.1016/j.coco.2020.100604.

Blondel, J., Joannès, S., Hervé-Luanco, E., 2020. Analytical modelling of the effect of morphological fluctuations on the transverse elastic behaviour of unidirectional fibre reinforced composites. Int. J. Sol. Struct. 206, 435–455. http://dx.doi.org/10.1016/j.ijsolstr.2020.06.001.

Böhm, H., 2019. Comparison of analytical and numerical models for the thermoelastic behavior of composites reinforced by coated spheres. Int. J. Eng. Sci. 142, 216–229. http://dx.doi.org/10.1016/j.ijengsci.2019.06.009.

Chatzigeorgiou, G., Meraghni, F., 2019. Elastic and inelastic local strain fields in composites with coated fibers or particles: Theory and validation. Math. Mech. Sol. 24, 2858–2894. http://dx.doi.org/10.1177/1081286518822695.

Chen, Q., Chatzigeorgiou, G., Meraghni, F., 2021. Hybrid hierarchical homogenization theory for unidirectional CNTs-coated fuzzy fiber composites undergoing inelastic deformations. Compos. Sci. Technol. 215, 109012. http://dx.doi.org/10.1016/j.compscitech.2021.109012.

Cherkaoui, M., Sabar, H., Berveiller, M., 1994. Micromechanical approach of the coated inclusion problem and applications to composite materials. J. Eng. Mater. Technol. 116, 274–278. http://dx.doi.org/10.1115/1.2904286.

Chouchaoui, C., Benzeggagh, M., 1997. The effect of interphase on the elastic behavior of a glass/epoxy bundle. Compos. Sci. Technol. 57, 617–622. http://dx.doi.org/10.1016/S0266-3538(96)00133-9.

Christensen, R., Lo, K., 1979. Solutions for effective shear properties in three phase sphere and cylinder models. J. Mech. Phys. Sol. 27, 315–330. http://dx.doi.org/10.1016/0022-5096(79)90032-2.

Dinzart, F., Sabar, H., Berbenni, S., 2016. Homogenization of multi-phase composites based on a revisited formulation of the multi-coated inclusion problem. Int. J. Eng. Sci. 100, 136–151. http://dx.doi.org/10.1016/j.ijengsci.2015.12.001.

Duan, H., Wang, J., Huang, Z., 2022. Micromechanics of composites with interface effects. Acta Mech. Sinica 38, 222025. http://dx.doi.org/10.1007/s10409-022-22025-x.

Dunn, M., Ledbetter, H., 1995. Elastic moduli of composites reinforced by multiphase particles. J. Appl. Mech. 62, 1023–1028. http://dx.doi.org/10.1115/1.2896038.

Dvorak, G., 1991. Plasticity theories for fibrous composite materials. In: Everett, R., Arsenault, R. (Eds.), Metal Matrix Composites: Mechanisms and Properties. Academic Press, Boston, MA, pp. 1–77.

Eshelby, J., 1957. The determination of the elastic field of an ellipsoidal inclusion and related problems. Proc. Roy. Soc. Lond. A241, 376–396. http://dx.doi.org/10.1098/rspa.1957.0133.

Firooz, S., Saeb, S., Chatzigeorgiou, G., Meraghni, F., Steinmann, P., Javili, A., 2019. Systematic study of homogenization and the utility of circular simplified representative volume element. Math. Mech. Sol. 24, 2961–2985. http://dx.doi.org/10.1177/1081286518823834.

Firooz, S., Steinmann, P., Javili, A., 2021. Homogenization of composites with extended general interfaces: Comprehensive review and unified modeling. Appl. Mech. Rev. 73, 040802. http://dx.doi.org/10.1115/1.4051481.

Friebel, C., Doghri, I., Legat, V., 2006. General mean-field homogenization schemes for viscoelastic composites containing multiple phases of coated inclusions. Int. J. Sol. Struct. 43, 2513–2541. http://dx.doi.org/10.1016/j.ijsolstr.2005.06.035.

Gardner, S., Pittman, C., Hackett, R., 1993. Polymeric composite materials incorporating an elastomeric interphase: A mathematical assessment. Compos. Sci. Technol. 46, 307–318. http://dx.doi.org/10.1016/0266-3538(93)90176-H.

Ghazavizadeh, A., Haboussi, M., Abdul-Latif, A., Jafari, A., Bousoura, H., 2019. A general and explicit eshelby-type estimator for evaluating the equivalent stiffness of multiply coated ellipsoidal heterogeneities. Int. J. Sol. Struct. 171, 103–116. http://dx.doi.org/10.1016/j.ijsolstr.2019.04.023.

Guinovart-Díaz, R., Rodríguez-Ramos, R., Bravo-Castillero, J., Sabina, F., Maugin, G., 2005. Closed form thermoelastic moduli of a periodic three-phase fiber-reinforced composite. J. Therm. Stresses 28, 1067–1093. http://dx.doi.org/10.1080/014957390967730.

Gusev, A., Kern, L., 2018. Frequency domain finite element estimates of viscoelastic stiffness of unidirectional composites. Compos. Struct. 194, 445–453. http://dx.doi.org/10.1016/j.compstruct.2018.02.027.

Hammerand, D., Seidel, G., Lagoudas, D., 2007. Computational micromechanics of clustering and interphase effects in carbon nanotube polymers. Mech. Adv. Mater. Struct. 14, 277–294. http://dx.doi.org/10.1080/15376490600817370.

Hashin, Z., 1965. On elastic behavior of fibre reinforced materials of arbitrary transverse phase geometry. J. Mech. Phys. Sol. 13, 119–134. http://dx.doi.org/10.1016/0022-5096(65)90015-3.

Hashin, Z., 1972. Theory of fiber reinforced materials. Technical Report, (NASA–CR–1974), NASA, Washington, DC.

Hashin, Z., 1983. Analysis of composite materials — A survey. J. Appl. Mech. 50, 481–505. http://dx.doi.org/10.1115/1.3167081.

Hashin, Z., 1988. The differential scheme and its application to cracked materials. J. Mech. Phys. Sol. 36, 719–733. http://dx.doi.org/10.1016/0022-5096(88)90005-1.

Hashin, Z., 1990. Thermoelastic properties of fiber composites with imperfect interface. Mech. Mater. 8, 333–348. http://dx.doi.org/10.1016/0167-6636(90)90027-D.

Hashin, Z., Rosen, B., 1964. The elastic moduli of fiber-reinforced materials. J. Appl. Mech. 31, 223–232. http://dx.doi.org/10.1115/1.3629590.

Hervé, E., Zaoui, A., 1995. Elastic behavior of multiply coated fibre-reinforced composites. Int. J. Eng. Sci. 33, 1419–1433. http://dx.doi.org/10.1016/0020-7225(95)00008-L.

Hervé-Luanco, E., 2020. Elastic behaviour of multiply coated fibre-reinforced composites: Simplification of the $(n+1)$-phase model and extension to imperfect interfaces. Int. J. Sol. Struct. 196–197, 10–25. http://dx.doi.org/10.1016/j.ijsolstr.2020.03.013.

Hill, R., 1952. The elastic behavior of a crystalline aggregate. Proc. Phys. Soc. Lond. A65, 349–354. http://dx.doi.org/10.1088/0370-1298/65/5/307.
Hill, R., 1963. Elastic properties of reinforced solids: Some theoretical principles. J. Mech. Phys. Sol. 11, 357–372. http://dx.doi.org/10.1016/0022-5096(63)90036-X.
Hill, R., 1965. Continuum micro-mechanics of elastoplastic polycrystals. J. Mech. Phys. Sol. 13, 89–101. http://dx.doi.org/10.1016/0022-5096(65)90023-2.
Hill, R., 1983. Interfacial operators in the mechanics of composite media. J. Mech. Phys. Sol. 31, 213–222. http://dx.doi.org/10.1016/0022-5096(83)90004-2.
Hori, M., Nemat-Nasser, S., 1993. Double-inclusion model and overall moduli of multi-phase composites. Mech. Mater. 14, 189–206. http://dx.doi.org/10.1016/0167-6636(93)90066-Z.
Jones, F., 2010. A review of interphase formation and design in fibre-reinforced composites. J. Adhesion Sci. Technol. 24, 171–202. http://dx.doi.org/10.1163/016942409X12579497420609.
Kanit, T., Forest, S., Galliet, I., Mounoury, V., Jeulin, D., 2003. Determination of the size of the representative volume element for random composites: Statistical and numerical approach. Int. J. Sol. Struct. 40, 3647–3679. http://dx.doi.org/10.1016/S0020-7683(03)00143-4.
Karger-Kocsis, J., Mahmood, H., Pegoretti, A., 2015. Recent advances in fiber/matrix interphase engineering for polymer composites. Prog. Mater. Sci. 73, 1–43. http://dx.doi.org/10.1016/j.pmatsci.2015.02.003.
Kari, S., Berger, H., Gabbert, U., Guinovart-Díaz, R., Bravo-Castillero, J., Rodriguez-Ramos, R., 2008. Evaluation of influence of interphase material parameters on effective material properties of three phase composites. Compos. Sci. Technol. 68, 684–691. http://dx.doi.org/10.1016/j.compscitech.2007.09.009.
Khoroshun, L., Leshchenko, P., Nazarenko, L., 1988. Effective thermoelastic constants of discretely-fibrous composites with anisotropic components. Int. Appl. Mech. 24, 955–961. http://dx.doi.org/10.1007/BF00901920.
Li, Y., Waas, A., Arruda, E., 2011. A closed-form, hierarchical, multi-interphase model for composites — Derivation, verification and application to nanocomposites. J. Mech. Phys. Sol. 59, 43–63. http://dx.doi.org/10.1016/j.jmps.2010.09.015.
Liu, W., Bian, L., 2019. A new energy-based effective strain theory for mechanical properties of multiphase composites. Eur. J. Mech. A 76, 279–289. http://dx.doi.org/10.1016/j.euromechsol.2019.04.015.
Livanov, K., Yang, L., Nissenbaum, A., Wagner, H., 2016. Interphase tuning for stronger and tougher composites. Sci. Rep. 6, 26305. http://dx.doi.org/10.1038/srep26305.
Michel, J., Moulinec, H., Suquet, P., 1999. Effective properties of composite materials with periodic microstructure: A computational approach. Comput. Meth. Appl. Mech. Eng. 172, 109–143. http://dx.doi.org/10.1016/S0045-7825(98)00227-8.
Moakher, M., Norris, A., 2006. The closest elastic tensor of arbitrary symmetry to an elastic tensor of lower symmetry. J. Elast. 85, 215–263. http://dx.doi.org/10.1007/s10659-006-9082-0.
Mogilevskaya, S., Crouch, S., Stolarski, H., Benusiglio, A., 2010. Equivalent inhomogeneity method for evaluating the effective elastic properties of unidirectional multi-phase composites with surface/interface effects. Int. J. Sol. Struct. 47, 407–418. http://dx.doi.org/10.1016/j.ijsolstr.2009.10.007.
Nazarenko, L., Stolarski, H., Altenbach, H., 2017. A model of cylindrical inhomogeneity with spring layer interphase and its application to analysis of short-fiber composites. Compos. Struct. 160, 635–652. http://dx.doi.org/10.1016/j.compstruct.2016.10.024.
Ostoja-Starzewski, M., 2006. Material spatial randomness: From statistical to representative volume element. Probab. Eng. Mech. 21, 112–131. http://dx.doi.org/10.1016/j.probengmech.2005.07.007.
Pagano, N., Tandon, G., 1988. Elastic response of multi-directional coated fiber composites. Compos. Sci. Technol. 31, 273–293. http://dx.doi.org/10.1016/0266-3538(88)90034-6.
Pitchai, P., Berger, H., Guruprasad, P., 2020. Investigating the influence of interface in a three phase composite using variational asymptotic method based homogenization technique. Compos. Struct. 233, 111562. http://dx.doi.org/10.1016/j.compstruct.2019.111562.
Ponte Castañeda, P., Willis, J., 1995. The effect of spatial distribution on the effective behavior of composite materials and cracked media. J. Mech. Phys. Sol. 43, 1919–1951. http://dx.doi.org/10.1016/0022-5096(95)00058-Q.
Ptashnyk, M., Seguin, B., 2016. Periodic homogenization and material symmetry in linear elasticity. J. Elast. 124, 225–241. http://dx.doi.org/10.1007/s10659-015-9566-x.
Riaño, L., Belec, L., Chailan, J., Joliff, Y., 2018. Effect of interphase region on the elastic behavior of unidirectional glass fiber/epoxy composites. Compos. Struct. 198, 109–116. http://dx.doi.org/10.1016/j.compstruct.2018.05.039.
Sager, R., Klein, P., Lagoudas, D., Zhang, Q., Liu, J., Dai, L., Baur, J., 2009. Effect of carbon nanotubes on the interfacial shear strength of T650 carbon fiber in an epoxy matrix. Compos. Sci. Technol. 69, 898–904. http://dx.doi.org/10.1016/j.compscitech.2008.12.021.
Schöberl, J., 1997. NETGEN — An advancing front 2D/3D-Mesh generator based on abstract rules. Comput. Visual Sci. 1, 41–52. http://dx.doi.org/10.1007/s00791005000.
Sevostianov, I., Rodríguez-Ramos, R., Guinovart-Díaz, R., Bravo-Castillero, J., Sabina, F., 2012. Connections between different models describing imperfect interfaces in periodic fiber-reinforced composites. Int. J. Sol. Struct. 49, 1518–1525. http://dx.doi.org/10.1016/j.ijsolstr.2012.02.028.
Theocaris, P., Varias, A., 1986. The influence of the mesophase on the transverse and longitudinal moduli and major Poisson ratio in fibrous composites. Colloid Polym. Sci. 264, 561–569. http://dx.doi.org/10.1007/BF01412593.
Torquato, S., 1998. Effective stiffness tensor of composite media: II. Applications to isotropic dispersions. J. Mech. Phys. Sol. 46, 1411–1440. http://dx.doi.org/10.1016/S0022-5096(97)00083-5.
Torquato, S., 2002. Random Heterogeneous Media. Springer-Verlag, New York, NY.
Torquato, S., Lado, F., 1992. Improved bounds on the effective moduli of random arrays of cylinders. J. Appl. Mech. 59, 1–6. http://dx.doi.org/10.1115/1.2899429.
Wang, B., Fang, G., Liu, S., Liang, J., 2019. Effect of heterogeneous interphase on the mechanical properties of unidirectional fiber composites studied by FFT-based method. Compos. Struct. 220, 642–651. http://dx.doi.org/10.1016/j.compstruct.2019.04.049.
Wang, Z., Oelkers, R., Lee, K., Fisher, F., 2016. Annular coated inclusion model and applications for polymer nancomposites — Part II: Cylindrical inclusions. Mech. Mater. 101, 50–60. http://dx.doi.org/10.1016/j.mechmat.2016.07.005.
Willis, J., 1977. Bounds and self-consistent estimates for the overall properties of anisotropic composites. J. Mech. Phys. Sol. 25, 185–202. http://dx.doi.org/10.1016/0022-5096(77)90022-9.
Zheng, H., Zhang, W., Li, B., Zhu, J., Wang, C., Song, G., Wu, G., Yang, X., Huang, Y., Ma, L., 2022. Recent advances of interphases in carbon fiber-reinforced polymer composites. Composites B 233, 109639. http://dx.doi.org/10.1016/j.compositesb.2022.109639.